

Massive MIMO Systems with Non-Ideal Hardware: Energy Efficiency, Estimation, and Capacity Limits

Emil Björnson, *Member, IEEE*, Jakob Hoydis, *Member, IEEE*, Marios Kountouris, *Member, IEEE*,
and Mérouane Debbah, *Senior Member, IEEE*

Abstract—The use of large-scale antenna arrays can bring substantial improvements in energy and/or spectral efficiency to wireless systems due to the greatly improved spatial resolution and array gain. Recent works in the field of massive multiple-input multiple-output (MIMO) show that the user channels decorrelate when the numbers of antennas at base stations (BSs) increase, thus strong signal gains are achievable with little inter-user interference. Since these results rely on asymptotics, it is important to investigate whether the conventional channel models are reasonable in the asymptotic regimes. This paper considers a new generalized channel model that incorporates transceiver hardware impairments at both the BSs (equipped with large antenna arrays) and the single-antenna user equipments (UEs). As opposed to the conventional case of ideal hardware, we show that hardware impairments create finite ceilings on the estimation accuracy and the downlink/uplink capacity of each user. Surprisingly, the capacity is mainly limited by the hardware at the UE, while the impact of impairments in the large-scale arrays vanishes asymptotically and inter-user interference (e.g., pilot contamination) becomes negligible. Furthermore, we prove that an arbitrarily high energy efficiency can be achieved by reducing the transmit power while increasing the number of antennas. Alternatively, a non-zero capacity can be retained while the hardware quality is decreased as the array grows, thus enabling the use of inexpensive antenna elements.

Index Terms—Capacity bounds, channel estimation, energy efficiency, massive MIMO, pilot contamination, time-division duplex, transceiver hardware impairments.

I. INTRODUCTION

The spectral efficiency of a wireless link is not only limited by the information-theoretic capacity [2], but also by the propagation environment [3], [4], channel estimation accuracy [5], transceiver hardware impairments [6], and signal processing complexity [7]. It is of profound importance to increase the spectral efficiency in future networks, to keep up with the increasing demand for wireless services. However, this is a

challenging task and usually comes at the price of having stricter hardware and overhead requirements.

A new network architecture has recently been proposed with the remarkable potential of both increasing the spectral efficiency and taking care of the aforementioned implementation issues. It is known as massive MIMO, or large-scale MIMO, and is based on having a very large number of antennas at each BS and exploiting channel reciprocity in time-division duplex (TDD) mode [7]–[11]. Some key features are: 1) propagation losses are mitigated by a large array gain due to coherent beamforming/combining; 2) interference-leakage due to channel estimation errors vanish asymptotically in the large-dimensional space; 3) low-complexity signal processing algorithms are asymptotically optimal; and 4) inter-user interference is easily mitigated by the high beamforming resolution.

The impact of transceiver hardware impairments on large-scale MIMO has received relatively little attention, although large arrays might only be attractive for network deployment if inexpensive hardware can be used at each antenna element. Cheap hardware components are particularly prone to the impairments (e.g., amplifier non-linearities [12], I/Q-imbalance [13], and phase noise [14]) that exist in any physical transceiver [14]–[18]. Transceiver impairments are known to fundamentally limit the capacity in the high-power regime [6], [19], while the behavior in the large antenna array regime is less known. To the best of our knowledge, the only previous works in this area are [20] which derives lower bounds on the achievable uplink sum rate for single-cell systems with phase noise and [21] which considers a constant-envelope precoding scheme that is robust to amplifier non-linearities.

This paper analyzes the *aggregate* impact of different hardware impairments on systems with large antenna arrays, in contrast to the ideal hardware considered in [8]–[11] and the single type of impairments considered in [20], [21]. Section II defines the generalized channel model with hardware impairments, which builds upon prior works in [14]–[18]. Section III derives a new pilot-based channel estimator and shows that the estimation accuracy is limited by the levels of impairments. The focus of Section IV is on a single link in the system where we derive lower and upper bounds on the downlink and uplink capacities. Our results reveal the existence of finite capacity ceilings due to hardware impairments. Despite these discouraging results, Section V shows that a very high energy efficiency and resilience towards hardware impairments at the BS can be achieved. Section VI puts these results in a multi-cell context and shows that inter-cell interference (including pilot contamination) basically drowns in the distortion noise

E. Björnson and M. Debbah are with the Alcatel-Lucent Chair on Flexible Radio, SUPELEC, Gif-sur-Yvette, France (e-mail: {emil.bjornson,merouane.debbah}@supelec.fr). E. Björnson is also with the Signal Processing Lab, ACCESS Linnaeus Centre, KTH Royal Institute of Technology, Stockholm, Sweden.

J. Hoydis is with Bell Laboratories, Alcatel-Lucent, Stuttgart, Germany (email: jakob.hoydis@alcatel-lucent.com).

M. Kountouris is with the Department of Telecommunications, SUPELEC, Gif-sur-Yvette, France (e-mail: marios.kountouris@supelec.fr).

This paper was presented in part at the International Conference on Digital Signal Processing (DSP), Santorini, Greece, July 2013 [1].

E. Björnson is funded by the International Postdoc Grant 2012-228 from The Swedish Research Council. This research has been supported by the ERC Starting Grant 305123 MORE (Advanced Mathematical Tools for Complex Network Engineering). Parts of this work have been performed in the framework of the FP7 project ICT-317669 METIS.

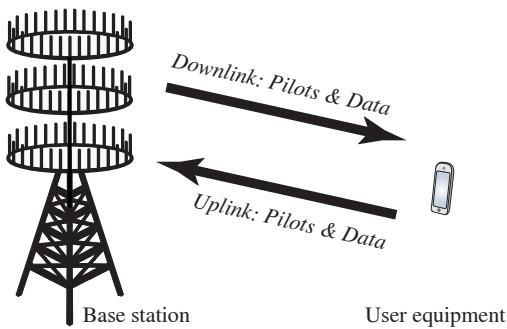


Fig. 1. Illustration of the TDD channel between a BS equipped with a large antenna array and a single-antenna UE.

from hardware impairments. Section VII describes the impact of various refinements of the channel model, while Section VIII summarizes the contributions and insights of the paper.

Notation: Boldface (lower case) is used for column vectors, \mathbf{x} , and (upper case) for matrices, \mathbf{X} . Let \mathbf{X}^T , \mathbf{X}^* , and \mathbf{X}^H denote the transpose, conjugate, and conjugate transpose of \mathbf{X} , respectively. $\mathbf{X}_1 \succeq \mathbf{X}_2$ means that $\mathbf{X}_1 - \mathbf{X}_2$ is positive semi-definite. A diagonal matrix with a_1, \dots, a_N on the main diagonal is denoted $\text{diag}(a_1, \dots, a_N)$ and \mathbf{I} denotes a identity matrix (of appropriate dimensions). The expectation operator is denoted $\mathbb{E}\{\cdot\}$. The Frobenius and spectral norms of a matrix \mathbf{X} are denoted by $\|\mathbf{X}\|_F$ and $\|\mathbf{X}\|_2$, respectively, while $\|\mathbf{x}\|_k$ denotes the L_k norm of a vector \mathbf{x} . A Gaussian random variable x is denoted $x \sim \mathcal{N}(\bar{x}, q)$, where \bar{x} is the mean and q is the variance. A circularly symmetric complex Gaussian random vector \mathbf{x} is denoted $\mathbf{x} \sim \mathcal{CN}(\bar{\mathbf{x}}, \mathbf{Q})$, where $\bar{\mathbf{x}}$ is the mean and \mathbf{Q} is the covariance matrix. The big \mathcal{O} notation $f(x) = \mathcal{O}(g(x))$ means that $\left| \frac{f(x)}{g(x)} \right|$ is bounded as $x \rightarrow \infty$.

II. CHANNEL AND SYSTEM MODEL

For analytical clarity, the majority of this paper analyzes the fundamental spectral and energy efficiency limits of a single link, which operates under arbitrary interference conditions. The link consists of an N -antenna BS and a single-antenna UE. A main characteristic in the analysis is that the number of antennas N can be very large. We consider a TDD protocol that toggles between uplink (UL) and downlink (DL) transmission on the same flat-fading subcarrier. This enables efficient channel estimation even when N is large, because the estimation accuracy in the UL is independent of N [7]. The acquired instantaneous channel state information (CSI) is utilized for DL and UL data transmission, by exploiting channel reciprocity;¹ see Fig. 1. In Section VI, we put our results in a multi-cell context with many users, inter-cell interference, and pilot contamination.

We assume a block fading structure where each channel is static for a *coherence period* of T_{coher} channel uses. The channel realizations are generated randomly and are independent between blocks. The TDD protocol is given in Fig. 2 and is based on [22], [23]. Each block begins with UL pilot/control signaling for $T_{\text{pilot}}^{\text{UL}}$ channel uses, followed by

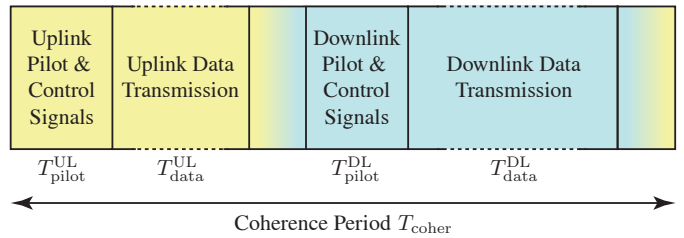


Fig. 2. Cyclic operation of a block-fading TDD system, where the coherence period T_{coher} is divided into phases for UL/DL pilot and data transmission.

UL data transmission for $T_{\text{data}}^{\text{UL}}$ channel uses. Next, the system toggles to the DL. This part begins with $T_{\text{pilot}}^{\text{DL}}$ channel uses of DL pilot/control signaling. These pilots are typically used by the UEs to estimate their effective channel (with precoding) and the current interference conditions, which enables coherent DL reception. Note that these are scalar quantities irrespective of N . The coherence period ends with DL data transmission for $T_{\text{data}}^{\text{DL}}$ channel uses. The four parameters must obviously satisfy $T_{\text{pilot}}^{\text{UL}} + T_{\text{data}}^{\text{UL}} + T_{\text{pilot}}^{\text{DL}} + T_{\text{data}}^{\text{DL}} \leq T_{\text{coher}}$, where the inequality is strict if guard intervals are required when switching between UL and DL. The analysis herein is valid for arbitrary fixed values on the four parameters, but we note that these can be optimized dynamically based on T_{coher} , user load, user conditions, ratio of UL/DL traffic, etc.

The stochastic channel between the BS and the UE is denoted $\mathbf{h} \in \mathbb{C}^{N \times 1}$. It is modeled as an ergodic process with a fixed independent realization $\mathbf{h} \sim \mathcal{CN}(\mathbf{0}, \mathbf{R})$ in each coherence period. This is known as Rayleigh block fading and $\mathbf{R} = \mathbb{E}\{\mathbf{h}\mathbf{h}^H\} \in \mathbb{C}^{N \times N}$ is the positive semi-definite covariance matrix. In the asymptotic analysis, we make the following technical assumptions:

- The spectral norm of \mathbf{R} is uniformly bounded, irrespective of the number of antennas N (i.e., $\|\mathbf{R}\|_2 = \mathcal{O}(1)$);
- The trace of \mathbf{R} scales linearly with N (i.e., $\text{tr}(\mathbf{R}) = \mathcal{O}(N)$) and \mathbf{R} has strictly positive diagonal elements.

The first assumption is a necessary physical property that originates from the law of energy conservation. It is also a common enabler for asymptotic analysis (cf. [10]). The second assumption is a typical consequence of increasing the array size with N and thereby improving the spatial resolution and aperture [7].² These assumptions imply $\liminf_N \frac{1}{N} \text{rank}(\mathbf{R}) > 0$, which basically means that $cN \leq \text{rank}(\mathbf{R}) \leq N$ for some $c > 0$. We stress that \mathbf{R} is generally *not* a scaled identity matrix, but describes the spatial propagation environment and might be rank-deficient (e.g., have a large conditional number) for large arrays due to insufficient richness of the scattering [3], [4].

A. Transceiver Hardware Impairments

The majority of papers on massive MIMO systems considers channels with ideal transceiver hardware. However, physical transceivers suffer from hardware impairments that 1) create a

¹The physical channels are always reciprocal, but different transceiver chains are typically used in the UL and DL. Careful calibration is therefore necessary to utilize the reciprocity for transmission; see Section VII-E.

²Although these assumptions make sense for practically large N [4], we cannot physically let $N \rightarrow \infty$ since the propagation environment is enclosed by a finite volume [7]. Nevertheless, our simulations reveal that the asymptotic analysis enabled by the technical assumptions is accurate at quite small N .

mismatch between the intended data signal and what is actually generated and emitted; and 2) distort the received signal in the reception processing. In this paper, we analyze how these impairments impact the performance and key asymptotic properties of massive MIMO systems. To this end, we consider a new generalized channel model from [14]–[18] that differs from the conventional model by having additive distortion noises at the BS as well as the UE. The details for the downlink and uplink are given in the next subsections.

B. Generalized Downlink Channel Model

The downlink channel is used for data transmission and pilot-based channel estimation; see Fig. 1. The received DL signal $y \in \mathbb{C}$ in a flat-fading multiple-input single-output (MISO) channel is conventionally modeled as

$$y = \mathbf{h}^T \mathbf{s} + n \quad (1)$$

where $\mathbf{s} \in \mathbb{C}^{N \times 1}$ is either a deterministic pilot symbol (during channel estimation) or a zero-mean stochastic data signal; in any case, the covariance matrix is denoted $\mathbf{W} = \mathbb{E}\{\mathbf{s}\mathbf{s}^H\}$ and the average power is $p^{\text{BS}} = \text{tr}(\mathbf{W})$. The additive term n is an independent ergodic process modeled as $n \sim \mathcal{CN}(0, \sigma^2)$. This term includes receiver noise with variance σ_{UE}^2 and interference from simultaneous data transmissions to other users; thus, the variance σ^2 might change between coherence periods, but it always satisfies $\sigma^2 \geq \sigma_{\text{UE}}^2$. It is only for brevity that we have a common notation for interference and receiver noise—it does not mean that the interference must be treated as noise at the receiver. A detailed interference model is provided in Section VI.

To model physical channels with non-ideal hardware more accurately, we consider a generalized channel model from [14]–[17] where the received signal at the UE is

$$y = \mathbf{h}^T (\mathbf{s} + \boldsymbol{\eta}_t^{\text{BS}}) + \eta_r^{\text{UE}} + n. \quad (2)$$

The difference from the conventional model in (1) is the additive distortion noise terms $\boldsymbol{\eta}_t^{\text{BS}} \sim \mathcal{CN}(\mathbf{0}, \boldsymbol{\Upsilon}_t^{\text{BS}})$ and $\eta_r^{\text{UE}} \sim \mathcal{CN}(0, v_r^{\text{UE}})$. These are independent and describe the impact of impairments in the transmitter and receiver hardware, respectively [14]. Theoretical investigations and many measurements have shown that the distortion noise caused an antenna is proportional to the signal power at this antenna, thus we have

$$\boldsymbol{\Upsilon}_t^{\text{BS}} = \kappa_t^{\text{BS}} p^{\text{BS}} \text{diag}(W_{11}, \dots, W_{NN}) \quad (3)$$

$$v_r^{\text{UE}} = \kappa_r^{\text{UE}} p^{\text{BS}} \mathbf{h}^T \mathbf{W} \mathbf{h}^* \quad (4)$$

where W_{ii} is the i th diagonal element of \mathbf{W} and $\kappa_t^{\text{BS}}, \kappa_r^{\text{UE}} \geq 0$ are the proportionality constants. The Gaussianity is explained by the aggregate effect of many impairments and the use of compensation algorithms that remove other types of distortions and structures [15], [16].

Remark 1. *Distortion noise is an alteration of the data signal, while the classical receiver noise models random fluctuations in the electronic circuits at the receiver. A main difference is thus that the distortion noise power is proportional to the signal power p^{BS} and the current channel gain $\|\mathbf{h}\|_2^2$. The*

proportionality constants κ_t^{BS} and κ_r^{UE} characterize the levels of impairments and are related to the error vector magnitude (EVM); for example, the EVM at the BS is defined as

$$\text{EVM}_t^{\text{BS}} = \sqrt{\frac{\mathbb{E}\{\|\boldsymbol{\eta}_t^{\text{BS}}\|_2^2\}}{\mathbb{E}\{\|\mathbf{s}\|_2^2\}}} = \sqrt{\frac{\text{tr}(\boldsymbol{\Upsilon}_t^{\text{BS}})}{\text{tr}(\mathbf{W})}} = \sqrt{\kappa_t^{\text{BS}}}. \quad (5)$$

The EVM is a common quality measure of transceivers and 3GPP LTE has EVM requirements in the range [0.08, 0.175], where high spectral efficiencies require small EVMs [24, Sec. 14.3.4]. Therefore, the κ -parameters in this paper are typically in the range [0, 0.15²] where small values represent accurate and expensive transceiver hardware.

The generalized channel model in (2) captures the main characteristics of non-ideal hardware, in the sense that it enables us to identify some fundamental differences in the behavior of massive MIMO systems as compared to the case of ideal hardware. The additive distortion noises can describe, for example, inter-carrier interference due to phase noise, leakage from the mirror subcarrier under I/Q imbalance, amplitude-amplitude nonlinearities in amplifiers, and quantization errors [14], [24], [25]. However, it cannot capture all characteristics of hardware impairments. Possible refinements, and their respective implications, are outlined in Section VII.

C. Generalized Uplink Channel Model

The reciprocal UL channel is used for pilot-based channel estimation and data transmission; see Fig. 1. Similar to (2), we consider a generalized model with the received signal $\mathbf{z} \in \mathbb{C}^N$ at the BS being

$$\mathbf{z} = \mathbf{h}(d + \eta_t^{\text{UE}}) + \boldsymbol{\eta}_r^{\text{BS}} + \boldsymbol{\nu} \quad (6)$$

where $d \in \mathbb{C}$ is either a deterministic pilot symbol (used for channel estimation) or a stochastic data signal; in any case, the average power is $p^{\text{UE}} = \mathbb{E}\{|d|^2\}$. The independent additive term $\boldsymbol{\nu} \in \mathbb{C}^{N \times 1}$ is an ergodic process that contains receiver noise with variance σ_{BS}^2 as well as potential interference from other simultaneous transmissions. The statistics might be different in the pilot and data transmission phases; for example, it is common to assume that each cell uses time-division multiple access (TDMA) in the pilot transmission, since this can provide sufficient CSI accuracy to enable spatial-division multiple access (SDMA) in the data transmission [7]–[11]. Therefore, we assume that $\boldsymbol{\nu} \sim \mathcal{CN}(\mathbf{0}, \mathbf{S})$ during pilot transmission and $\boldsymbol{\nu} \sim \mathcal{CN}(\mathbf{0}, \mathbf{Q})$ in the data transmission. The covariance matrices $\mathbf{S}, \mathbf{Q} \in \mathbb{C}^{N \times N}$ are positive definite. We assume that \mathbf{S} has a uniformly bounded spectral norm, $\|\mathbf{S}\|_2 = \mathcal{O}(1)$, for the same physical reasons as for \mathbf{R} . The spectral norm of \mathbf{Q} might however grow unboundedly with N which can give rise to pilot contamination in multi-cell scenarios [7]–[11]; see Section VI for further details.

The transceiver impairments in the hardware used for UL transmission are modeled by the independent distortion noises $\eta_t^{\text{UE}} \sim \mathcal{CN}(0, v_t^{\text{UE}})$ and $\boldsymbol{\eta}_r^{\text{BS}} \sim \mathcal{CN}(\mathbf{0}, \boldsymbol{\Upsilon}_r^{\text{BS}})$ at the transmitter and receiver, respectively. Similar to (3) and (4), their

covariance matrices are model as

$$v_t^{\text{UE}} = \kappa_t^{\text{UE}} p^{\text{UE}} \quad (7)$$

$$\mathbf{\Upsilon}_r^{\text{BS}} = \kappa_r^{\text{BS}} p^{\text{UE}} \text{diag}(|h_1|^2, \dots, |h_N|^2). \quad (8)$$

Note that the hardware quality is characterized by $\kappa_t^{\text{BS}}, \kappa_r^{\text{BS}}$ at the BS and by $\kappa_t^{\text{UE}}, \kappa_r^{\text{UE}}$ at the UE. We might have $\kappa_t^{\text{BS}} \neq \kappa_r^{\text{BS}}$ and $\kappa_t^{\text{UE}} \neq \kappa_r^{\text{UE}}$ since different transceiver chains are used for transmission and reception at a device.

Generally speaking, we would like to achieve high performance using cheap hardware. This is particularly evident in massive MIMO systems since the deployment cost of large antenna arrays might scale linearly with N unless we can accept higher levels of impairments, $\kappa_t^{\text{BS}}, \kappa_r^{\text{BS}}$, at the BSs than in conventional systems. This is analyzed in Section V.

III. UPLINK CHANNEL ESTIMATION

This section considers estimation of the current channel realization \mathbf{h} by comparing the received UL signal \mathbf{z} in (6) with the predefined UL pilot signal d (recall: $p^{\text{UE}} = |d|^2$). The classic results on pilot-based channel estimation consider Rayleigh fading channels that are observed in independent complex Gaussian noise with known statistics [26]–[29]. However, this is not the case herein because the distortion noises η_t^{UE} and η_r^{BS} effectively depend on the unknown random channel \mathbf{h} . The dependence is either through the multiplication $\mathbf{h}\eta_t^{\text{UE}}$ or the conditional variance of η_r^{BS} in (8), which is essentially the same relation. Although the distortion noises are Gaussian when conditioned on a channel realization, the effective distortion is the product of Gaussian variables and, thus, has a *complex double Gaussian* distribution [30].³ Consequently, an optimal channel estimator cannot be deduced from the standard results provided in [26]–[29].

We now derive the *linear* minimum mean square error (LMMSE) estimator of \mathbf{h} under hardware impairments.

Theorem 1. *The LMMSE estimator of \mathbf{h} from the observation of \mathbf{z} in (6) is*

$$\hat{\mathbf{h}} = \underbrace{d^* \mathbf{R} \bar{\mathbf{Z}}^{-1}}_{\triangleq \mathbf{A}} \mathbf{z} \quad (9)$$

where $\mathbf{R}_{\text{diag}} = \text{diag}(r_{11}, \dots, r_{NN})$ consists of the diagonal elements of \mathbf{R} and the covariance matrix of \mathbf{z} is denoted as

$$\bar{\mathbf{Z}} = \mathbb{E}\{\mathbf{z}\mathbf{z}^H\} = p^{\text{UE}}(1 + \kappa_t^{\text{UE}})\mathbf{R} + p^{\text{UE}}\kappa_r^{\text{BS}}\mathbf{R}_{\text{diag}} + \mathbf{S}. \quad (10)$$

The total MSE is $\text{MSE} = \mathbb{E}\{\|\hat{\mathbf{h}} - \mathbf{h}\|_2^2\} = \text{tr}(\mathbf{C})$, where the error covariance matrix is

$$\mathbf{C} = \mathbb{E}\{(\hat{\mathbf{h}} - \mathbf{h})(\hat{\mathbf{h}} - \mathbf{h})^H\} = \mathbf{R} - p^{\text{UE}}\mathbf{R}\bar{\mathbf{Z}}^{-1}\mathbf{R}. \quad (11)$$

Proof: The LMMSE estimator has the form $\hat{\mathbf{h}} = \mathbf{A}\mathbf{z}$ where \mathbf{A} minimizes the MSE. The MSE definition gives

$$\text{MSE} = \text{tr}\left(\mathbf{R} - d\mathbf{A}\mathbf{R} - d^*\mathbf{R}\mathbf{A}^H + \mathbf{A}\bar{\mathbf{Z}}\mathbf{A}^H\right) \quad (12)$$

³For example, the i th element of η_r^{BS} can be expressed as $x_i = h_i\xi_i$, which is the product of the i th channel coefficient $h_i \sim \mathcal{CN}(0, r_{ii})$ and an independent variable $\xi_i \sim \mathcal{CN}(0, \kappa_r^{\text{BS}}p^{\text{UE}})$. The joint product distribution is complex double Gaussian with the PDF $f(x_i) = \frac{2}{\pi\mu_i}K_0\left(2\frac{|x_i|}{\sqrt{\mu_i}}\right)$, where $\mu_i = r_{ii}\kappa_r^{\text{BS}}p^{\text{UE}}$ is the variance and $K_0(\cdot)$ denotes the zeroth-order modified Bessel function of the second kind [30].

where the expectations that involve $\eta_t^{\text{UE}}, \eta_r^{\text{BS}}$ in $\text{MSE} = \mathbb{E}\{\|\hat{\mathbf{h}} - \mathbf{h}\|_2^2\}$ are computed by first having a fixed value of \mathbf{h} and then average over \mathbf{h} . The LMMSE estimator in (9) is achieved by differentiation of (12) with respect to \mathbf{A} and equating to zero. The error covariance matrix and MSE are obtained by plugging (9) into the respective definitions. ■

Based on Theorem 1, the channel can be decomposed as $\mathbf{h} = \hat{\mathbf{h}} + \epsilon$ where $\hat{\mathbf{h}}$ is the LMMSE estimate in (9) and $\epsilon \in \mathbb{C}^{N \times 1}$ denotes the unknown estimation error. Contrary to conventional estimation with independent Gaussian noise (cf. [26, Chapter 15.8]), $\hat{\mathbf{h}}$ and ϵ are neither independent nor jointly complex Gaussian, but only uncorrelated and zero-mean. The covariance matrices are $\mathbb{E}\{\hat{\mathbf{h}}\hat{\mathbf{h}}^H\} = \mathbf{R} - \mathbf{C}$ and $\mathbb{E}\{\epsilon\epsilon^H\} = \mathbf{C}$ where \mathbf{C} was given in (11).

We remark that there might exist non-linear estimators that achieve smaller MSEs than the LMMSE estimator in Theorem 1. This stands in contrast to conventional channel estimation with independent Gaussian noise, where the LMMSE estimator is also the MMSE estimator [28]. However, the difference in MSE performance should be small, since the dependent distortion noises are relatively weak.

Corollary 1. *Consider the special case of $\mathbf{R} = \lambda\mathbf{I}$ and $\mathbf{S} = \sigma_{\text{BS}}^2\mathbf{I}$. The error covariance matrix in (11) becomes*

$$\mathbf{C} = \lambda \left(1 - \frac{p^{\text{UE}}\lambda}{p^{\text{UE}}\lambda(1 + \kappa_t^{\text{UE}} + \kappa_r^{\text{BS}}) + \sigma_{\text{BS}}^2}\right) \mathbf{I}. \quad (13)$$

In the high UL power regime, we have

$$\lim_{p^{\text{UE}} \rightarrow \infty} \mathbf{C} = \lambda \left(1 - \frac{1}{1 + \kappa_t^{\text{UE}} + \kappa_r^{\text{BS}}}\right) \mathbf{I}. \quad (14)$$

This corollary brings important insights on the average estimation error per element in \mathbf{h} . The error variance is given by the factor in front of the identity matrix in (13). It is independent of the number of antennas N , thus letting N grow large neither increases nor decreases the estimation error *per element*.⁴ The estimation error is clearly a decreasing function of the pilot power $p^{\text{UE}} = |d|^2$, but contrary to the ideal hardware case the error variance is *not* converging to zero as $p^{\text{UE}} \rightarrow \infty$. As seen in (14), there is a strictly positive error floor of $\lambda(1 - \frac{1}{1 + \kappa_t^{\text{UE}} + \kappa_r^{\text{BS}}})$ due to transceiver hardware impairments. Thus, perfect estimation accuracy cannot be achieved in practice, not even asymptotically. The error floor is characterized by the sum of the levels of impairments $\kappa_t^{\text{UE}}, \kappa_r^{\text{BS}}$ in the transmitter and receiver hardware, respectively. In terms of estimation accuracy, it is thus equally important to have high-quality hardware at the BS and at the UE.

There is an error floor also for non-diagonal covariance matrices \mathbf{R} and \mathbf{S} ; the general high-power limit is easily computed from (11). The observations above also hold for any zero-mean channel and noise distributions with covariance matrices \mathbf{R} and \mathbf{S} , since the LMMSE estimator and MSE only exploit the first two moments of the statistics [26], [28].

⁴The MSE per element is finite, i.e. $\frac{1}{N}\text{tr}(\mathbf{C}) < \infty$, but the sum MSE behaves as $\text{tr}(\mathbf{C}) \rightarrow \infty$ when $N \rightarrow \infty$ since the number of elements grows.

A. Impact of Pilot Length

The LMMSE estimator in Theorem 1 considers a scalar pilot signal d , which is sufficient to excite all channel dimensions. With ideal hardware and a total pilot power constraint, a scalar pilot signal is then sufficient to minimize the MSE [28]. We now show that this property does not hold for non-ideal hardware.

Suppose we use a pilot signal $\mathbf{d} \in \mathbb{C}^{1 \times B}$ that spans $1 \leq B \leq T_{\text{pilot}}^{\text{UL}}$ channel uses. A simple estimation approach would be to compute B separate LMMSE estimates $\hat{\mathbf{h}}_i = \mathbf{h} - \epsilon_i$, for $i = 1, \dots, B$, using Theorem 1. By averaging, we then obtain

$$\hat{\mathbf{h}} = \frac{1}{B} \sum_{i=1}^B \hat{\mathbf{h}}_i = \mathbf{h} - \frac{1}{B} \sum_{i=1}^B \epsilon_i. \quad (15)$$

If the distortion noises are temporally uncorrelated and identically distributed, the MSE of the estimate $\hat{\mathbf{h}}$ is

$$\mathbb{E} \left\{ \left(\frac{1}{B} \sum_{i=1}^B \epsilon_i \right)^H \left(\frac{1}{B} \sum_{j=1}^B \epsilon_j \right) \right\} = \frac{\text{tr}(\mathbf{C})}{B} \quad (16)$$

and thus it goes to zero as $1/B$ when the pilot length B is increased. The diminishing MSE in (16) for $B \rightarrow \infty$ stands in contrast to the non-zero MSE floor demonstrated in Corollary 1 for $B = 1$.

To comprehend the difference, recall that the reason for the non-zero MSE floor is that the total distortion noise power is proportional to the total pilot power. If the same pilot power is spread over B channel uses instead, we obtain B noise observations which average out by the law of large numbers if they are uncorrelated. Nevertheless, the estimation accuracy is limited by the finite coherence period (i.e., $B \leq T_{\text{coher}}$). Furthermore, the distortion might be temporally correlated in practice, especially if the same pilot symbol d is used multiple times. In these cases, one can obtain better MSEs by estimating \mathbf{h} jointly from all the B observations.

Finding the B that maximizes some measure of system-wide throughput is also of great interest, but this is outside the scope of our current paper. We refer to [28], [29], [31], [32] for some relevant works in the case of ideal hardware.

B. Numerical Illustrations

This section exemplifies the impact of hardware impairments on the channel estimation accuracy.

In Fig. 3, we consider $N = 50$ antennas at the BS, no interference, and a receiver noise covariance of $\mathbf{S} = \mathbf{I}$. The channel covariance matrix \mathbf{R} is generated by the exponential correlation model from [33], which means that the i, j th element of \mathbf{R} is

$$[\mathbf{R}]_{i,j} = \begin{cases} \delta r^{j-i}, & i \leq j, \\ \delta (r^{i-j})^*, & i > j, \end{cases} \quad (17)$$

where δ is an arbitrary scaling factor. This model basically describes a uniform linear array (ULA) where the correlation between adjacent antennas is given by the coefficient r with $|r| \leq 1$. We consider a correlation coefficient of $r = 0.7$, which can be seen as a modest correlation [34]. Fig. 3 shows

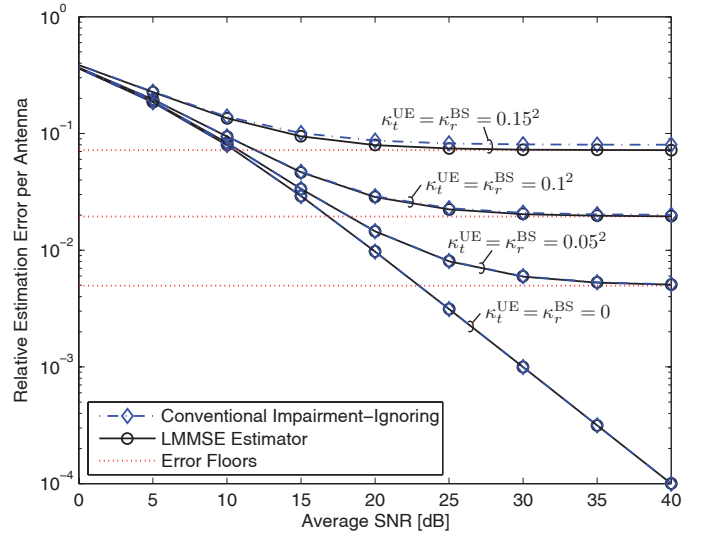


Fig. 3. Estimation error per antenna element for the LMMSE estimator in Theorem 1 and the conventional impairment-ignoring MMSE estimator. Transceiver hardware impairments create non-zero error floors.

the relative estimation error per channel element, $\frac{\text{MSE}}{\text{tr}(\mathbf{R})}$, as a function of the average SNR in the UL, defined as

$$\text{SNR}^{\text{UL}} = p^{\text{UE}} \frac{\text{tr}(\mathbf{R})}{\text{tr}(\mathbf{S})}. \quad (18)$$

Four hardware setups with different levels of impairments are considered: $\kappa_t^{\text{UE}} = \kappa_r^{\text{BS}} \in \{0, 0.05^2, 0.1^2, 0.15^2\}$. We compare the LMMSE estimator in Theorem 1 with the conventional impairment-ignoring MMSE estimator from [26]–[28]. The curves are generated by our analytical expressions, while the marker symbols are obtained by Monte Carlo simulations.⁵

Fig. 3 confirms that there are non-zero error floors at high SNRs, as proved by Corollary 1 and the subsequent discussion. The error floor increases with the levels of impairments. The estimation error is very close to the floor when the uplink SNR reaches 20–30 dB, thus further increase in SNR only brings minor improvement. Moreover, Fig. 3 shows that the conventional impairment-ignoring estimator is only slightly worse than the proposed LMMSE estimator. This indicates that although hardware impairments greatly affect the estimation performance, it only brings minor changes to the structure of the optimal estimator.

Next, we illustrate the improvement in estimation accuracy by increasing the pilot length to comprise $B \geq 1$ channel uses. As discussed in Section III-A, it is not clear whether the distortion noise is temporally uncorrelated or correlated in practice. Therefore, we fix the levels of impairments at $\kappa_t^{\text{UE}} = \kappa_r^{\text{BS}} = 0.05^2$ and consider the two extremes: temporally uncorrelated and fully correlated distortion noises. The latter means that the distortion noise realizations are the same for all B channel uses, since the pilot is always distorted in the same way. The channel and receiver noise statistics are generated as in the previous figure (i.e., $N = 50$, $\mathbf{S} = \mathbf{I}$, and \mathbf{R} from exponential correlation model with $r = 0.7$).

⁵Note that the MSE of any linear estimator $\tilde{\mathbf{A}}\mathbf{z}$ can be computed by plugging the matrix $\tilde{\mathbf{A}}$ into the general MSE expression in (12). The difference in MSE is easily quantified by comparing with $\text{tr}(\mathbf{C})$ using (11).

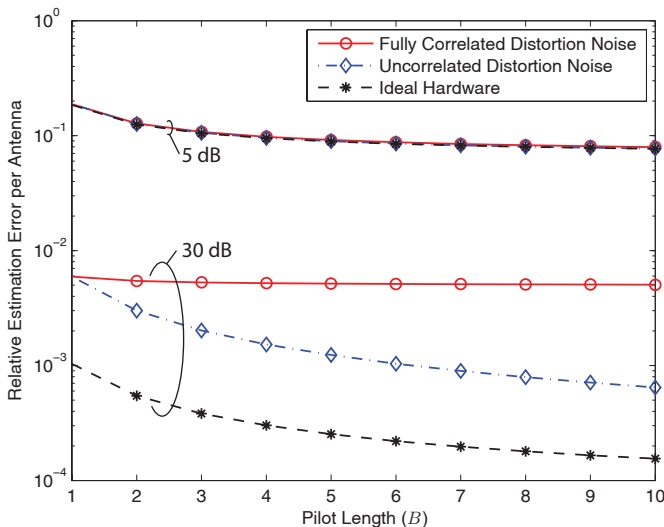


Fig. 4. Estimation error per antenna element for the LMMSE estimator in Theorem 1 as a function of the pilot length B . The levels of impairments are $\kappa_t^{\text{UE}} = \kappa_r^{\text{BS}} = 0.05^2$ and different temporal correlations are considered.

The relative estimation error per antenna element is shown in Fig. 4 as a function of the pilot length. We also show the performance with ideal hardware as a reference. At a low SNR of 5 dB, hardware impairments have little impact and there is a small but clear gain from increasing the pilot length because the total pilot power increases as Bp^{UE} . At a high SNR of 30 dB, the temporal correlation has a large impact. Only small improvements are possible in the fully correlated case, since only the receiver noise can be averaged out by increasing B . In the uncorrelated case the distortion noise can be also mitigated by increasing B . This gives a logarithmic slope similar to the case of ideal hardware. We stress that the actual performance lies somewhere in between the two extremes.

Next, we consider different channel covariance models:

- 1) Uncorrelated antennas $\mathbf{R} = \mathbf{I}$. (Equivalent to the exponential correlation model in (17) with $r = 0$.)
- 2) Exponential correlation model with $r = 0.7$.
- 3) One-ring model with 20 degrees angular spread [35].
- 4) One-ring model with 10 degrees angular spread [35].

The exponential correlation model was defined in (17) above. The classic one-ring model assumes a ring of scatterers around the UE, while there is no scattering close to the BS [35]. From the BS perspective, the multipath components arrive from a main angle of arrival (here: 30 degrees) and a small angular spread around it (here: 10 or 20 degrees). The BS is assumed to have a ULA with half-wavelength antenna spacings. An important property of this model is that \mathbf{R} might not have full rank as N grows large [36], [37], due to insufficient scattering.

The relative estimation error per channel element is shown in Fig. 5 for these four channel covariance models. We consider two SNRs (5 and 30 dB), hardware impairments with $\kappa_t^{\text{UE}} = \kappa_r^{\text{BS}} = 0.05^2$, and show the estimation errors as a function of the number of BS antennas. The main observation from Fig. 5 is that the choice of covariance model has a large impact on the estimation accuracy. It was proved in [28] that spatially correlated channels are easier to estimate which is consistent with our results; increasing the coefficient r in

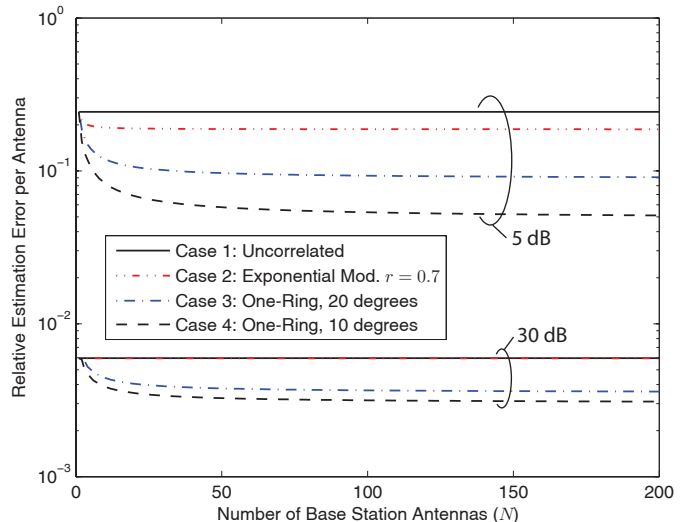


Fig. 5. Estimation error per antenna element for the LMMSE estimator in Theorem 1 as a function of the number of BS antennas. Four different channel covariance models are considered and $\kappa_t^{\text{UE}} = \kappa_r^{\text{BS}} = 0.05^2$.

the exponential correlation model and decreasing the angular spread in the one-ring model lead to higher spatial correlation and smaller errors in Fig. 5. However, the error floors due to hardware impairments make the differences between the models reduce with the SNR. Moreover, the estimation error *per* antenna is virtually independent of N in the exponential correlation model, while increasing N improves the error *per* antenna in the one-ring model. This is explained by the limited richness of the propagation environment in the one-ring model, which is a physical property that we can expect in practice as well. Finally, we note that it becomes increasingly difficult to obtain consistent estimates of the covariance matrices \mathbf{R} and \mathbf{S} as N grows large [38]. With imperfectly estimated covariance matrices, the estimation error per antenna might increase for large arrays since the covariance matrices are essential when computing the LMMSE estimate in (9). The quantification of this degradation is an open problem. The large-dimensional matrix inversion in (9) is also computationally expensive, but alternatives based on polynomial expansions have been proposed [39].

IV. DOWNLINK AND UPLINK DATA TRANSMISSION

This section analyzes the ergodic channel capacities of the downlink in (2) and the uplink in (6), under the fixed TDD protocol in Fig. 2. We begin with defining these capacities.

We consider the ergodic capacity (in bits/channel use) of the generalized memoryless DL channel in (2) under imperfect channel knowledge. The BS selects the distribution $f(\mathbf{s})$ of the data signal based on some instantaneous knowledge of the channel \mathbf{h} . The UE has a separate statistical characterization of \mathbf{h} and $f(\mathbf{s})$, obtained from the long-term statistics and possibly some additional DL pilot signaling. We leave the extent of CSI at the BS and UE undefined since the bounds derived in this section hold for anything between simple UL pilot signaling with no DL pilot signaling and perfect channel estimation at both sides. Based on the well-known capacity expressions in

[40], the ergodic capacity is

$$\mathsf{C}^{\text{DL}} = \frac{T_{\text{data}}^{\text{DL}}}{T_{\text{coher}}} \mathbb{E} \left\{ \max_{f(\mathbf{s}) : \mathbb{E}\{\|\mathbf{s}\|_2^2\} \leq p^{\text{BS}}} \mathcal{I}(\mathbf{s}; y) \right\} \quad (19)$$

where $\mathcal{I}(\mathbf{s}; y)$ denotes the mutual information between the received signal y and data signal \mathbf{s} in the DL. Note that the factor $T_{\text{data}}^{\text{DL}}/T_{\text{coher}}$ is the fixed fraction of channel uses allocated for DL data transmission.

In addition, the ergodic capacity (in bits/channel use) of the generalized memoryless fading UL channel in (6) is

$$\mathsf{C}^{\text{UL}} = \frac{T_{\text{data}}^{\text{UL}}}{T_{\text{coher}}} \mathbb{E} \left\{ \max_{f(d) : \mathbb{E}\{|d|^2\} \leq p^{\text{UE}}} \mathcal{I}(d; \mathbf{z}) \right\} \quad (20)$$

where $\mathcal{I}(d; \mathbf{z})$ denotes the mutual information between the received signal \mathbf{z} and data signal d in the UL. The probability distribution of the data signal is denoted $f(d)$. The fraction of channel uses allocated for UL data transmission is $T_{\text{data}}^{\text{UL}}/T_{\text{coher}}$.

We characterize the capacities in this section by deriving lower and upper bounds on (19) and (20). The expectations in (19) and (20) are taken over coherence periods with static values on \mathbf{h} and the CSI at each side. The covariances σ^2 and \mathbf{Q} can also change between coherence periods, since the corresponding terms include inter-user interference in addition to receiver noise. The lower bounds treat the interference as noise, while the upper bounds suppress the interference perfectly—thus exploiting that $\sigma^2 \geq \sigma_{\text{UE}}^2$ and $\mathbf{Q} \succeq \sigma_{\text{BS}}^2 \mathbf{I}$ where $\sigma_{\text{UE}}^2, \sigma_{\text{BS}}^2$ are the receiver noise variances. Section VI analyzes the interference in multi-cell scenarios in detail.

We assume that the distortion noises are temporally uncorrelated, which is a good model when the data signals are also temporally uncorrelated. Moreover, we study the capacity behavior in the limit of infinitely many BS antennas ($N \rightarrow \infty$), which bring insights on how hardware impairments affect links with large antenna arrays. The DL and UL are analyzed side-by-side since the results follow from similar derivations.

A. Upper Bounds on Channel Capacities

Upper bounds on the capacities in (19) and (20) can be obtained by removing all interference and adding extra CSI. We assume that the UL/DL pilot signals provide the BS and UE with perfect knowledge of \mathbf{h} in each coherence period. Since the noise and distortion noises in (2) and (6) are circular symmetric complex Gaussian and independent of the useful signals under perfect CSI, we deduce that single-stream Gaussian signaling is optimal in the DL and UL [2], [6]; that is, $\mathbf{s} = \mathbf{w}s$ for $s \sim \mathcal{CN}(0, p^{\text{BS}})$ and some unit-norm beamforming vector \mathbf{w} in the DL and $d \sim \mathcal{CN}(0, p^{\text{UE}})$ in the UL. This gives us the following initial upper bounds.

Lemma 1. *The downlink and uplink capacities in (19) and*

(20), respectively, are bounded as

$$\mathsf{C}^{\text{DL}} \leq \frac{T_{\text{data}}^{\text{DL}}}{T_{\text{coher}}} \times \quad (21)$$

$$\mathbb{E} \left\{ \log_2 \left(1 + \mathbf{h}^H \left(\kappa_t^{\text{BS}} \mathbf{D}_{|\mathbf{h}|^2} + \kappa_r^{\text{UE}} \mathbf{h} \mathbf{h}^H + \frac{\sigma_{\text{UE}}^2}{p^{\text{BS}}} \mathbf{I} \right)^{-1} \mathbf{h} \right) \right\}$$

$$\mathsf{C}^{\text{UL}} \leq \frac{T_{\text{data}}^{\text{UL}}}{T_{\text{coher}}} \times \quad (22)$$

$$\mathbb{E} \left\{ \log_2 \left(1 + \mathbf{h}^H \left(\kappa_t^{\text{UE}} \mathbf{h} \mathbf{h}^H + \kappa_r^{\text{BS}} \mathbf{D}_{|\mathbf{h}|^2} + \frac{\sigma_{\text{BS}}^2}{p^{\text{UE}}} \mathbf{I} \right)^{-1} \mathbf{h} \right) \right\}$$

where $\mathbf{D}_{|\mathbf{h}|^2} = \text{diag}(|h_1|^2, \dots, |h_N|^2)$ with $\mathbf{h} = [h_1 \dots h_N]^T$. These upper bounds are achieved with equality under perfect CSI, using the beamforming vector

$$\mathbf{w}_{\text{upper}}^{\text{DL}} = \frac{(\kappa_t^{\text{BS}} \mathbf{D}_{|\mathbf{h}|^2} + \frac{\sigma_{\text{UE}}^2}{p^{\text{BS}}} \mathbf{I})^{-1} \mathbf{h}^*}{\|(\kappa_t^{\text{BS}} \mathbf{D}_{|\mathbf{h}|^2} + \frac{\sigma_{\text{UE}}^2}{p^{\text{BS}}} \mathbf{I})^{-1} \mathbf{h}^*\|_2} \quad (23)$$

in the downlink and by applying a receive combining vector

$$\mathbf{w}_{\text{upper}}^{\text{UL}} = \frac{(\kappa_r^{\text{BS}} \mathbf{D}_{|\mathbf{h}|^2} + \frac{\sigma_{\text{BS}}^2}{p^{\text{UE}}} \mathbf{I})^{-1} \mathbf{h}}{\|(\kappa_r^{\text{BS}} \mathbf{D}_{|\mathbf{h}|^2} + \frac{\sigma_{\text{BS}}^2}{p^{\text{UE}}} \mathbf{I})^{-1} \mathbf{h}\|_2}. \quad (24)$$

in the uplink.⁶

Proof: The proof is given in Appendix B-A. ■

Note that the beamforming vector in (23) and receive combining vector in (24) only depend on the channel vector \mathbf{h} , hardware impairments at the BS, and the receiver noise. Hardware impairments at the UE have no impact on $\mathbf{w}_{\text{upper}}^{\text{DL}}$ and $\mathbf{w}_{\text{upper}}^{\text{UL}}$ since they essentially act as an interferer with the same channel as the data signal, thus filtering cannot reduce it.

The bounds in Lemma 1 are not amenable to simple analysis, but the lemma enables us to derive further bounds on the channel capacities that are in closed form.

Theorem 2. *The downlink and uplink capacities in (19) and (20), respectively, are bounded as*

$$\mathsf{C}^{\text{DL}} \leq \mathsf{C}_{\text{upper}}^{\text{DL}} = \frac{T_{\text{data}}^{\text{DL}}}{T_{\text{coher}}} \log_2 \left(1 + \frac{G^{\text{DL}}}{1 + \kappa_r^{\text{UE}} G^{\text{DL}}} \right) \quad (25)$$

$$\mathsf{C}^{\text{UL}} \leq \mathsf{C}_{\text{upper}}^{\text{UL}} = \frac{T_{\text{data}}^{\text{UL}}}{T_{\text{coher}}} \log_2 \left(1 + \frac{G^{\text{UL}}}{1 + \kappa_t^{\text{UE}} G^{\text{UL}}} \right) \quad (26)$$

where r_{11}, \dots, r_{NN} are the diagonal elements of \mathbf{R} ,

$$G^{\text{DL}} = \sum_{i=1}^N \frac{1}{\kappa_t^{\text{BS}}} \left(1 - \frac{\sigma_{\text{UE}}^2 e^{\frac{\sigma_{\text{BS}}^2}{p^{\text{BS}} \kappa_t^{\text{BS}} r_{ii}}}}{p^{\text{BS}} \kappa_t^{\text{BS}} r_{ii}} E_1 \left(\frac{\sigma_{\text{UE}}^2}{p^{\text{BS}} \kappa_t^{\text{BS}} r_{ii}} \right) \right), \quad (27)$$

$$G^{\text{UL}} = \sum_{i=1}^N \frac{1}{\kappa_r^{\text{BS}}} \left(1 - \frac{\sigma_{\text{BS}}^2 e^{\frac{\sigma_{\text{UE}}^2}{p^{\text{UE}} \kappa_r^{\text{BS}} r_{ii}}}}{p^{\text{UE}} \kappa_r^{\text{BS}} r_{ii}} E_1 \left(\frac{\sigma_{\text{BS}}^2}{p^{\text{UE}} \kappa_r^{\text{BS}} r_{ii}} \right) \right), \quad (28)$$

and $E_1(x) = \int_1^\infty \frac{e^{-tx}}{t} dt$ denotes the exponential integral.

⁶A receive combining vector \mathbf{w} is a linear filter $\mathbf{w}^H \mathbf{z}$ that transforms the system into an effective single-input single-output (SISO) channel.

Proof: The proof is given in Appendix B-B. ■

These closed-form upper bounds provide important insights on the achievable DL and UL performance under transceiver impairments. In particular, the following two corollaries provide some ultimate capacity limits in the asymptotic regimes of many BS antennas or large transmit powers.

Corollary 2. *The downlink upper capacity bound in (25) has the following asymptotic properties:*

$$\lim_{p^{\text{BS}} \rightarrow \infty} \mathsf{C}_{\text{upper}}^{\text{DL}} = \frac{T_{\text{data}}^{\text{DL}}}{T_{\text{coher}}} \log_2 \left(1 + \frac{N}{\kappa_t^{\text{BS}} + \kappa_r^{\text{UE}} N} \right) \quad (29)$$

$$\lim_{N \rightarrow \infty} \mathsf{C}_{\text{upper}}^{\text{DL}} = \frac{T_{\text{data}}^{\text{DL}}}{T_{\text{coher}}} \log_2 \left(1 + \frac{1}{\kappa_r^{\text{UE}}} \right). \quad (30)$$

Proof: The diagonal elements of \mathbf{R} satisfy $r_{ii} > 0 \forall i$, by definition, thus $G^{\text{DL}} \rightarrow \sum_{i=1}^N \frac{1}{\kappa_t^{\text{BS}}} = \frac{N}{\kappa_t^{\text{BS}}}$ as $p^{\text{BS}} \rightarrow \infty$ for fixed N , giving (29). The positive diagonal elements also implies $\frac{1}{N} G^{\text{DL}} > 0$ as $N \rightarrow \infty$, thus $\frac{G^{\text{DL}}}{1 + \kappa_r^{\text{UE}} G^{\text{DL}}} - \frac{G^{\text{DL}}}{\kappa_r^{\text{UE}} G^{\text{DL}}} \rightarrow 0$ as $N \rightarrow \infty$ which turns (25) into (30). ■

This corollary shows that the DL capacity has finite ceilings when either the DL transmit power p^{BS} or the number of BS antennas N grow large. The ceilings depend on the impairment parameters κ_t^{BS} and κ_r^{UE} , but the UE impairments are clearly N times more influential. Note that even very small hardware impairments will ultimately limit the capacity. In other words, the ever-increasing capacity observed in the high-SNR and large- N regimes with ideal transceiver hardware (cf. [7], [9]–[11]) is not easily achieved in practice.

The next corollary provides analogous results for the UL.

Corollary 3. *The uplink upper capacity bound in (26) has the following asymptotic properties:*

$$\lim_{p^{\text{UE}} \rightarrow \infty} \mathsf{C}_{\text{upper}}^{\text{UL}} = \frac{T_{\text{data}}^{\text{UL}}}{T_{\text{coher}}} \log_2 \left(1 + \frac{N}{\kappa_r^{\text{BS}} + \kappa_t^{\text{UE}} N} \right) \quad (31)$$

$$\lim_{N \rightarrow \infty} \mathsf{C}_{\text{upper}}^{\text{UL}} = \frac{T_{\text{data}}^{\text{UL}}}{T_{\text{coher}}} \log_2 \left(1 + \frac{1}{\kappa_t^{\text{UE}}} \right). \quad (32)$$

Proof: This is proved analogously to Corollary 2. ■

As seen from Corollary 3, the UL capacity also has finite ceilings when either the UL transmit power p^{UE} or the number of antennas N grow large. Analogous to the DL, the UE impairments are N times more influential than the BS impairments.

Remark 2 (BS Impairments Vanish Asymptotically). *The asymptotic bounds (30) and (32) indicate that only the quality of the UE's transceiver hardware limits the DL and UL capacities as $N \rightarrow \infty$. Thus, the detrimental effect of hardware impairments at the BS vanishes when the number of BS antennas grows large. This is, simply speaking, since the BS's distortion noises are spread in some arbitrary direction in space while the increased spatial resolution of the array enables very exact transmit beamforming and receive combining for the useful signal. This is a very promising result since large arrays are more prone to impairments, due implementation limitations and the will to deploy antenna elements of lower quality (to avoid having deployment costs that increase linearly with N). In contrast, the UE's distortion noises are non-vanishing since*

these behave as interferers with the same effective channels as the useful signals.

To verify the observations in Remark 2, we also need lower bounds on the channel capacities.

B. Lower Bounds on Channel Capacities

We obtain lower capacity bounds by making the potentially limiting assumptions of Gaussian codebooks, treating interference as noise, linear single-stream beamforming in the DL, linear receive combining in the UL, pilot-based channel estimation as in Theorem 1, and entropy-maximizing Gaussian CSI uncertainty at the receiver of the DL and UL.⁷ The next theorem is obtained by an approach from [5], which has been applied to massive MIMO systems in [9]–[11] (among others).

Theorem 3. *Let \mathcal{B}^{UE} and \mathcal{B}^{BS} denote the CSI available in the decoding at the receiver in the downlink and uplink, respectively. The downlink and uplink capacities in (19) and (20), respectively, are then bounded as*

$$\mathsf{C}^{\text{DL}} \geq \mathsf{C}_{\text{lower}}^{\text{DL}} = \frac{T_{\text{data}}^{\text{DL}}}{T_{\text{coher}}} \mathbb{E} \left\{ \log_2 \left(1 + \text{SINR}_{\text{lower}}^{\text{DL}}(\mathbf{v}^{\text{DL}}) \right) \right\} \quad (33)$$

$$\mathsf{C}^{\text{UL}} \geq \mathsf{C}_{\text{lower}}^{\text{UL}} = \frac{T_{\text{data}}^{\text{UL}}}{T_{\text{coher}}} \mathbb{E} \left\{ \log_2 \left(1 + \text{SINR}_{\text{lower}}^{\text{UL}}(\mathbf{v}^{\text{UL}}) \right) \right\} \quad (34)$$

where the beamforming vector $\mathbf{v}^{\text{DL}} = [v_1^{\text{DL}} \dots v_{K_r}^{\text{DL}}]^T$ and the receive combining vector $\mathbf{v}^{\text{UL}} = [v_1^{\text{UL}} \dots v_{K_r}^{\text{UL}}]^T$ are functions of $\hat{\mathbf{h}}$ and have unit norm. The expectations are taken over \mathcal{B}^{UE} and \mathcal{B}^{BS} , while the SINR expressions for DL and UL are given in (35) and (36), respectively, at the top of the next page.

Proof: The proof is given in Appendix B-C. ■

The lower bounds in (33) and (34) can be computed numerically for any channel distribution and any way of selecting the beamforming vector (in the DL) and receiver combining vector (in the UL) from the channel estimate, provided that the joint conditional distribution of $(\mathbf{h}, \hat{\mathbf{h}})$ given \mathcal{B} can be characterized.⁸ To bring insights on the behavior when the number of antennas, N , grows large, we have the following result for the cases of (approximate) maximum ratio transmission (MRT) in the DL and (approximate) maximum ratio combining (MRC) in the UL.

Theorem 4. *Assume that no instantaneous CSI is utilized for decoding (i.e., $\mathcal{B}^{\text{BS}} = \mathcal{B}^{\text{UE}} = \emptyset$). For $\mathbf{v} = \frac{\hat{\mathbf{h}}}{\|\hat{\mathbf{h}}\|_2}$ the terms in (35) and (36) behave as*

$$|\mathbb{E}\{\mathbf{h}^H \mathbf{v}\}|^2 = |\mathbb{E}\{\varphi\}|^2 \text{tr}(\mathbf{R} - \mathbf{C}) + \mathcal{O}(\sqrt{N}) \quad (37)$$

$$\mathbb{E}\{|\mathbf{h}^H \mathbf{v}|^2\} = \mathbb{E}\{|\varphi|^2\} \text{tr}(\mathbf{R} - \mathbf{C}) + \mathcal{O}(\sqrt{N}) \quad (38)$$

$$\sum_{i=1}^N \mathbb{E}\{|h_i|^2 |v_i|^2\} = \mathcal{O}(1) \quad (39)$$

where

$$\varphi = \frac{(1 + d^{-1} \eta_t^{\text{UE}}) \sqrt{\text{tr}(\mathbf{R} - \mathbf{C})}}{\sqrt{\text{tr}(\mathbf{A}(|d + \eta_t^{\text{UE}}|^2 \mathbf{R} + \mathbf{\Psi}) \mathbf{A}^H)}} \quad (40)$$

⁷The linear processing assumptions are motivated by its asymptotic optimality as $N \rightarrow \infty$ [7].

⁸Finding such a characterization is not an easy task, except for the case $\mathcal{B}^{\text{BS}} = \mathcal{B}^{\text{UE}} = \emptyset$ considered in Theorem 4.

$$\text{SINR}_{\text{lower}}^{\text{DL}}(\mathbf{v}^{\text{DL}}) = \frac{|\mathbb{E}\{\mathbf{h}^H \mathbf{v}^{\text{DL}} | \mathcal{B}^{\text{UE}}\}|^2}{(1 + \kappa_r^{\text{UE}}) \mathbb{E}\{|\mathbf{h}^H \mathbf{v}^{\text{DL}}|^2 | \mathcal{B}^{\text{UE}}\} - |\mathbb{E}\{\mathbf{h}^H \mathbf{v}^{\text{DL}} | \mathcal{B}^{\text{UE}}\}|^2 + \kappa_t^{\text{BS}} \sum_{i=1}^N \mathbb{E}\{|h_i|^2 | v_i^{\text{DL}}|^2 | \mathcal{B}^{\text{UE}}\} + \frac{\mathbb{E}\{\sigma^2 | \mathcal{B}^{\text{UE}}\}}{p^{\text{BS}}}} \quad (35)$$

$$\text{SINR}_{\text{lower}}^{\text{UL}}(\mathbf{v}^{\text{UL}}) = \frac{|\mathbb{E}\{\mathbf{h}^H \mathbf{v}^{\text{UL}} | \mathcal{B}^{\text{BS}}\}|^2}{(1 + \kappa_t^{\text{UE}}) \mathbb{E}\{|\mathbf{h}^H \mathbf{v}^{\text{UL}}|^2 | \mathcal{B}^{\text{BS}}\} - |\mathbb{E}\{\mathbf{h}^H \mathbf{v}^{\text{UL}} | \mathcal{B}^{\text{BS}}\}|^2 + \kappa_r^{\text{BS}} \sum_{i=1}^N \mathbb{E}\{|h_i|^2 | v_i^{\text{UL}}|^2 | \mathcal{B}^{\text{BS}}\} + \frac{\mathbb{E}\{(\mathbf{v}^{\text{UL}})^H \mathbf{Q} \mathbf{v}^{\text{UL}} | \mathcal{B}^{\text{BS}}\}}{p^{\text{UE}}}} \quad (36)$$

is a function of the random variable η_t^{UE} while $\mathbf{A} = d^* \mathbf{R} \bar{\mathbf{Z}}^{-1}$ and $\Psi = p^{\text{UE}} \kappa_r^{\text{BS}} \mathbf{R}_{\text{diag}} + \mathbf{S}$ are deterministic matrices.

Proof: The proof is given in Appendix B-D. ■

Similar asymptotic behaviors were derived in [9]–[11] for the case of ideal hardware.⁹ In the general case with hardware impairments, the expectations of φ and $|\varphi|^2$ must be computed numerically, because the randomness of the scalar distortion noise η_t^{UE} at the UE remains even when N grows large. In the special case of $\kappa_t^{\text{UE}} = 0$ (which implies $\eta_t^{\text{UE}} = 0$), (37) and (38) both reduce to $\text{tr}(\mathbf{R} - \mathbf{C}) + \mathcal{O}(\sqrt{N})$. Nevertheless, the terms in Theorem 4 can be computed efficiently.

For the downlink, we provide the following capacity characterizations that enables asymptotic analysis.

Corollary 4. Consider the DL with beamforming vector $\mathbf{v} = \frac{\hat{\mathbf{h}}^*}{\|\hat{\mathbf{h}}\|_2}$ and $\mathcal{B}^{\text{UE}} = \emptyset$. If $\mathbb{E}\{\sigma^2\} \leq \mathcal{O}(N^n)$ for some $n < 1$, the lower capacity bound in (33) can be expressed as

$$\mathcal{C}^{\text{DL}} \geq \frac{T_{\text{data}}^{\text{DL}}}{T_{\text{coher}}} \times \log_2 \left(1 + \frac{|\mathbb{E}\{\varphi\}|^2 + \mathcal{O}\left(\frac{1}{\sqrt{N}}\right)}{(1 + \kappa_r^{\text{UE}}) \mathbb{E}\{|\varphi|^2\} - |\mathbb{E}\{\varphi\}|^2 + \mathcal{O}\left(\frac{1}{\sqrt{N}} + \frac{1}{N^{1-n}}\right)} \right) \quad (41)$$

where φ is given in (40). The terms $\mathcal{O}\left(\frac{1}{\sqrt{N}}\right)$ and $\mathcal{O}\left(\frac{1}{N^{1-n}}\right)$ vanish when $N \rightarrow \infty$, while the other terms are strictly positive in the limit.

Proof: The expression (41) is obtained from (33) by plugging in the expressions in Theorem 4 and dividing each term by $\text{tr}(\mathbf{R} - \mathbf{C}) = p^{\text{UE}} \text{tr}(\mathbf{R} \bar{\mathbf{Z}}^{-1} \mathbf{R}) = \mathcal{O}(N)$. The noise term becomes $\frac{\mathbb{E}\{\sigma^2\}}{p^{\text{BS}} \text{tr}(\mathbf{R} - \mathbf{C})} = \mathcal{O}\left(\frac{1}{N^{1-n}}\right)$. ■

Combining the upper bound in Corollary 2 with the lower bound in Corollary 4, we have a clear characterization of the DL capacity behavior when $N \rightarrow \infty$. Both bounds are independent of κ_t^{BS} in the limit, thus the transmitter hardware of the BS plays little role in massive MIMO systems. Contrary to the upper bound, the level of receiver hardware impairments at the BS (κ_r^{BS}) is present in the lower bound (41), through \mathbf{A} and Ψ in φ . However, our numerical results reveal that the asymptotic impact of BS impairments is negligible also in

⁹We stress that the assumption in Theorem 4 that decoding is performed without instantaneous CSI is only made to enable closed-form lower bounds. The BS should certainly exploit the channel estimate $\hat{\mathbf{h}}$ and the UE might receive a downlink pilot signal that enables estimation of the effective channel $\mathbf{h}^H \mathbf{v}^{\text{DL}}$. While this is relatively easy to handle with ideal hardware, where the channel estimate and estimation error are independent (cf. [10]), the extension to non-ideal hardware seems intractable due the statistical dependence between the channel estimate and estimation error.

the lower bound. This can also be seen analytically in certain cases; if $\kappa_t^{\text{UE}} = 0$ we get $\varphi = 1$ and therefore

$$\lim_{N \rightarrow \infty} \mathcal{C}_{\text{lower}}^{\text{DL}} = \frac{T_{\text{data}}^{\text{DL}}}{T_{\text{coher}}} \log_2 \left(1 + \frac{1}{\kappa_r^{\text{UE}}} \right). \quad (42)$$

In this special case, the lower bound actually equals the upper bound in (30) asymptotically, and any DL capacity can be achieved by making κ_r^{UE} sufficiently small. The opposite is not true; setting $\kappa_r^{\text{BS}} = 0$ will *not* make the impact of UE impairments vanish. We therefore conclude that the DL capacity limit is mainly determined by the level of impairments at the UE, both in the uplink estimation (κ_t^{UE}) and the downlink transmission (κ_r^{UE})—although the former connection was not visible in the upper bound since it assumed perfect CSI.

For the uplink, we have the following similar capacity characterization.

Corollary 5. Consider the UL with receive combining vector $\mathbf{v} = \frac{\hat{\mathbf{h}}}{\|\hat{\mathbf{h}}\|_2}$ and $\mathcal{B}^{\text{BS}} = \emptyset$. If $\mathbb{E}\{\|\mathbf{Q}\|_2\} \leq \mathcal{O}(N^n)$ for some $n < 1$, the lower capacity bound in (34) can be expressed as

$$\mathcal{C}^{\text{UL}} \geq \frac{T_{\text{data}}^{\text{UL}}}{T_{\text{coher}}} \times \log_2 \left(1 + \frac{|\mathbb{E}\{\varphi\}|^2 + \mathcal{O}\left(\frac{1}{\sqrt{N}}\right)}{(1 + \kappa_t^{\text{UE}}) \mathbb{E}\{|\varphi|^2\} - |\mathbb{E}\{\varphi\}|^2 + \mathcal{O}\left(\frac{1}{\sqrt{N}} + \frac{1}{N^{1-n}}\right)} \right) \quad (43)$$

where φ is given in (40). The terms $\mathcal{O}\left(\frac{1}{\sqrt{N}}\right)$ and $\mathcal{O}\left(\frac{1}{N^{1-n}}\right)$ vanish when $N \rightarrow \infty$, while the other terms are strictly positive in the limit.

Proof: The expression (43) is obtained from (34) by plugging in the expressions in Theorem 4 and dividing each term by $\text{tr}(\mathbf{R} - \mathbf{C}) = p^{\text{UE}} \text{tr}(\mathbf{R} \bar{\mathbf{Z}}^{-1} \mathbf{R}) = \mathcal{O}(N)$. The noise term becomes $\frac{\mathbb{E}\{\mathbf{v}^H \mathbf{Q} \mathbf{v}\}}{p^{\text{UE}} \text{tr}(\mathbf{R} - \mathbf{C})} = \mathcal{O}\left(\frac{1}{N^{1-n}}\right)$. ■

The upper bound in Corollary 3 and the lower bound in Corollary 5 provide a joint characterization of the uplink capacity when N grows large. The UE impairments manifest the behavior in both bounds; the BS impairments are present in (41) since φ depends on \mathbf{A} and Ψ , but their impact vanish when $\kappa_t^{\text{UE}} \rightarrow 0$. By making κ_t^{UE} appropriately small, we can thus achieve any UL capacity as N grows large. We therefore conclude that it is of main importance to have high quality hardware at the UE, which is analog to our observations for the DL. These observations are illustrated numerically in the next section.

The properties $\mathbb{E}\{\sigma^2\} \leq \mathcal{O}(N^n)$ and $\mathbb{E}\{\|\mathbf{Q}\|_2\} \leq \mathcal{O}(N^n)$ for some $n < 1$ were assumed in Corollaries 4 and 5,

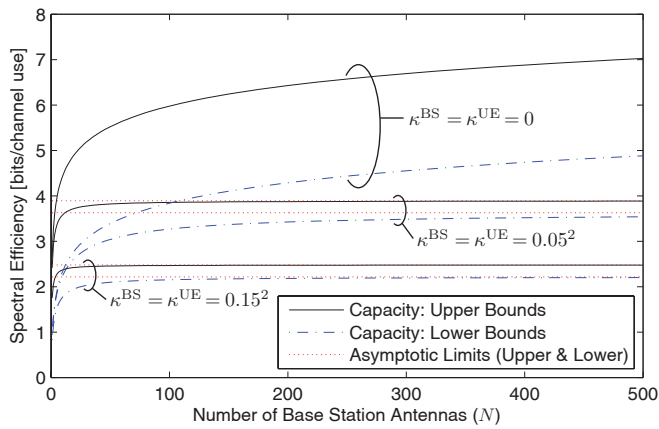


Fig. 6. Lower and upper bounds on the capacity. Hardware impairments have a fundamental impact on the asymptotic behavior as N grows large.

respectively. These imply that the noise terms only vanish asymptotically if the scaling with N is slower than linear. This is satisfied by receiver noise (for a fixed hardware setup) and regular interference (which gives $n = 0$), but there is a special type of pilot contaminated interference in multi-cell systems that scales linearly with N . This adds an additional non-vanishing term to the denominators of (41) and (43). We detail this scenario in Section VI.

Finally, we stress that the DL and UL capacity bounds in Corollaries 2 and 3, respectively, have a very similar structure. The main difference is that the UL is only affected by UL impairments (i.e., $\kappa_t^{\text{UE}}, \kappa_r^{\text{BS}}$), while the DL is affected by both DL and UL impairments (i.e., all κ -parameters) due to the reverse-link channel estimation.

C. Numerical Illustrations

This section illustrates the lower and upper bounds on the capacity that was derived earlier in this section. The average SNR is defined as $p \frac{\text{tr}(\mathbf{R})}{\text{tr}(\mathbf{Q})}$ and $p \frac{\text{tr}(\mathbf{R})}{N\sigma^2}$ in the UL and DL, respectively, and is fixed at 20 dB, while we vary the number of antennas N and the levels of impairments. For simplicity, we assume $\mathbf{Q} = \mathbf{S} = \mathbf{I}$, $\sigma^2 = 1$, and let $\kappa^{\text{BS}} \triangleq \kappa_t^{\text{BS}} = \kappa_r^{\text{BS}}$ at the BS and $\kappa^{\text{UE}} \triangleq \kappa_t^{\text{UE}} = \kappa_r^{\text{UE}}$ at the UE. Furthermore, $\frac{T_{\text{data}}^{\text{DL}}}{T_{\text{coher}}} = \frac{T_{\text{data}}^{\text{UL}}}{T_{\text{coher}}} = 0.45$. These parameter values make the bounds for the DL and UL capacities become identical.

Fig. 6 considers a spatially uncorrelated scenario with $\mathbf{R} = \mathbf{I}$. The capacity with ideal hardware grows without bound as $N \rightarrow \infty$, while the lower and upper bounds converge to finite limits under transceiver hardware impairments. Recall that these bounds hold under any CSI conditions at the BS and UE; the lower bounds represent no CSI in the decoding step and the upper bounds represent perfect CSI. Although the gap between these extremes is large for ideal hardware, the difference is remarkably small under non-ideal hardware due to the finite capacity limit and the channel hardening that makes random inner product such as $\mathbf{h}^H \mathbf{v}$ become increasingly deterministic as N grows large.

The asymptotic capacity limits in Fig. 6 are characterized by the level of impairments, thus the hardware quality has a fundamental impact on the achievable spectral efficiency. The majority of the multi-antenna gain is achieved at relatively low

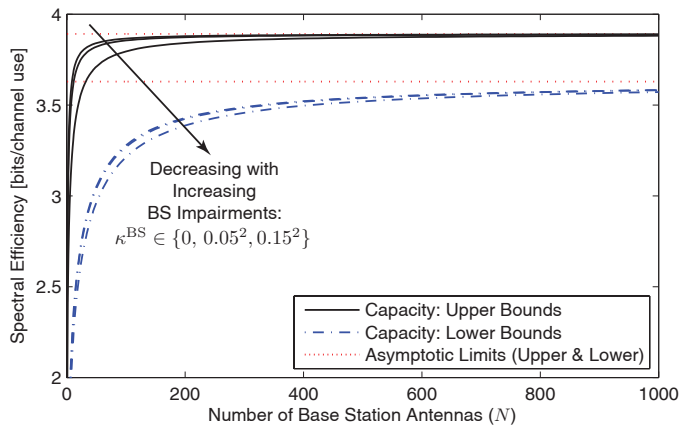


Fig. 7. Lower and upper bounds on the capacity for $\kappa^{\text{UE}} = 0.05^2$. The impact of hardware impairments at the BS vanishes asymptotically.

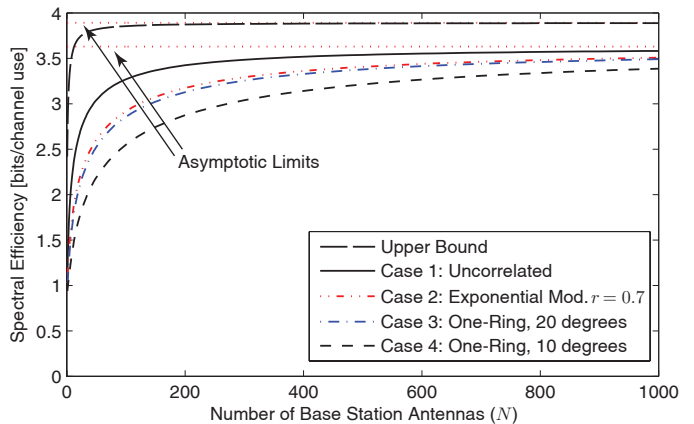


Fig. 8. Lower and upper bounds on the capacity as a function of the number of BS antennas. Four different channel covariance models are considered and $\kappa^{\text{BS}} = \kappa^{\text{UE}} = 0.05$.

N ; in particular, only minor improvements can be achieved by having more than $N = 100$ antennas. Larger numbers can however be useful for inter-user interference suppression and multiplexing; see Section VI.

Next, Fig. 7 considers the same scenario as in Fig. 6 but with a fixed level of impairments $\kappa^{\text{UE}} = 0.05^2$ at the UE and different values at the BS. As expected from the analysis, the lower and upper capacity bounds increase with κ^{BS} , but the difference is only visible at small N since the curves converge to virtually the same value as $N \rightarrow \infty$. This validates that the impact of impairments at the BS vanishes as N grows large.

Finally, we consider the capacity behavior for different channel covariance models, namely the four propagation scenarios described in Section III-B. The lower and upper capacity bounds are shown in Fig. 8 for $\kappa^{\text{BS}} = \kappa^{\text{UE}} = 0.05$. The upper bound is identical for all the models, since it only utilizes the diagonal elements of \mathbf{R} . However, there are clear differences between the lower bounds. The spatially uncorrelated covariance model provides the highest performance, while the strongly spatially correlated one-ring model from [35] with 10 degrees angular spread gives the lowest performance. This stands in contrast to Section III-B, where the highly correlated channels gave the lowest estimation errors. We note, however, that the differences between the channel covariance models vanish asymptotically.

V. IMPROVING ENERGY EFFICIENCY AND REDUCING HARDWARE QUALITY

The large array gain in massive MIMO systems can be utilized for power reductions and thereby increased energy efficiency, as shown for ideal hardware in [10], [11] and phase noise-impaired uplink systems in [20]. This section extends this line of work to our generalized channel model with hardware impairments. Furthermore, we show that the hardware quality at the BS can be relaxed as N grows large.

Similar to [11], [41], we define the energy efficiency (in bits/Joule) as the ratio of spectral efficiency (in bits/channel use) to emitted power (in Joules/channel use).

Definition 1. *The downlink energy efficiency is*

$$\text{EE}^{\text{DL}} = \frac{\mathcal{C}^{\text{DL}}}{\left(\frac{T_{\text{data}}^{\text{DL}}}{T_{\text{coher}}} + \alpha_1\right) p^{\text{BS}} + \alpha_2 p^{\text{UE}}} \quad (44)$$

and the uplink energy efficiency is

$$\text{EE}^{\text{UL}} = \frac{\mathcal{C}^{\text{UL}}}{\left(\frac{T_{\text{data}}^{\text{UL}}}{T_{\text{coher}}} + \alpha_3\right) p^{\text{UE}}} \quad (45)$$

where $\alpha_1, \alpha_2, \alpha_3 \geq 0$ are constants related to the overhead signaling needed for downlink and uplink transmission. The EE of any suboptimal transmission scheme is computed by replacing the capacities \mathcal{C}^{DL} and \mathcal{C}^{UL} with the corresponding achievable spectral efficiencies.

The α -parameters model the required overhead signaling. The parameter α_1 should typically be proportional to $T_{\text{pilot}}^{\text{DL}}/T_{\text{coher}}$, while α_2 and α_3 should be proportional to $T_{\text{pilot}}^{\text{UL}}/T_{\text{coher}}$. The proportionality makes sure that the power spent on DL/UL overhead signaling in one coherence period is spread equally over the channel uses of data transmission and all the UEs served in the cell (if there are more than one UE).

Recall from Corollaries 2 and 3 that the downlink and uplink capacities have finite ceilings as $N \rightarrow \infty$ or $p^{\text{UE}}, p^{\text{BS}} \rightarrow \infty$. This means that high energy efficiency cannot be achieved by only increasing the number of antennas or the transmit powers. However, we have the following important result, which has counterparts for ideal hardware in [10], [11] and phase noise-impaired uplink systems in [20].

Corollary 6. *Suppose the downlink transmit power p^{BS} and uplink pilot power p^{UE} are reduced proportionally to $1/N^{t_{\text{BS}}}$ and $1/N^{t_{\text{UE}}}$, respectively. If $t_{\text{BS}} + t_{\text{UE}} < 1$, $t_{\text{BS}} \geq 0, 0 < t_{\text{UE}} < \frac{1}{2}$, and $\mathbb{E}\{\sigma^2\} = \mathcal{O}(1)$, the lower bound in Corollary 4 satisfies*

$$\lim_{N \rightarrow \infty} \mathcal{C}^{\text{DL}} \geq \frac{T_{\text{data}}^{\text{DL}}}{T_{\text{coher}}} \log_2 \left(1 + \frac{1}{\kappa_r^{\text{UE}} + \kappa_t^{\text{UE}} + \kappa_r^{\text{UE}} \kappa_t^{\text{UE}}} \right). \quad (46)$$

Similarly, suppose the uplink transmit/pilot power p^{UE} is reduced proportionally to $1/N^{t_{\text{UE}}}$. If $0 < t_{\text{UE}} < \frac{1}{2}$ and $\mathbb{E}\{\|\mathbf{Q}\|_2\} = \mathcal{O}(1)$, the lower bound in Corollary 5 satisfies

$$\lim_{N \rightarrow \infty} \mathcal{C}^{\text{UL}} \geq \frac{T_{\text{data}}^{\text{UL}}}{T_{\text{coher}}} \log_2 \left(1 + \frac{1}{2\kappa_t^{\text{UE}} + (\kappa_t^{\text{UE}})^2} \right). \quad (47)$$

Proof: The proof is given in Appendix B-E. ■

Corollary 6 shows that one can reduce the downlink and uplink powers as N grows large (e.g., roughly proportionally to $1/\sqrt{N}$) and obtain non-zero capacities; the downlink capacity is lower bounded by (46) and the uplink capacity by (47). The conditions $\mathbb{E}\{\sigma^2\} = \mathcal{O}(1)$ and $\mathbb{E}\{\|\mathbf{Q}\|_2\} = \mathcal{O}(1)$ are stronger than the ones in Corollaries 4 and 5, thus interfering transmissions might have to reduce their powers in the same way as in Corollary 6.

As expected from Section IV, the lower bounds only depend on the levels of impairments at the UE. Furthermore, the power scaling in Corollary 6 has the extraordinary consequences

$$\begin{aligned} \lim_{N \rightarrow \infty} \text{EE}^{\text{DL}} &= \lim_{N \rightarrow \infty} \frac{\mathcal{C}^{\text{DL}}}{\left(\frac{T_{\text{data}}^{\text{DL}}}{T_{\text{coher}}} + \alpha_1\right) \frac{p^{\text{BS}}}{N^{t_{\text{BS}}}} + \alpha_2 \frac{p^{\text{UE}}}{N^{t_{\text{UE}}}}} = \infty \\ \lim_{N \rightarrow \infty} \text{EE}^{\text{UL}} &= \lim_{N \rightarrow \infty} \frac{\mathcal{C}^{\text{UL}}}{\left(\frac{T_{\text{data}}^{\text{UL}}}{T_{\text{coher}}} + \alpha_3\right) \frac{p^{\text{UE}}}{N^{t_{\text{UE}}}}} = \infty. \end{aligned} \quad (48)$$

Observe that these unbounded asymptotic energy efficiencies are achieved by using the LMMSE estimator in Theorem 1 for uplink channel estimation and simple linear processing at the BS (approximate MRT in the DL and MRC in the UL). Massive MIMO systems can thus obtain an immense energy efficiency even under transceiver hardware impairments.

Remark 3. *Although the ratio of capacity to emitted power in Definition 1 can grow unboundedly as shown in (48), the overall energy efficiency (spectral efficiency divided by total power consumption) will generally not. More specifically, each antenna that is added to the system requires dedicated circuits that have a non-zero power consumption $\varrho > 0$ [Joule/channel use]. To model the total power consumption, there should also be a static circuit power term $\zeta > 0$ [Joule/channel use] that describes baseband processing and other overhead power consumption that are not scaling with N .¹⁰ The power terms $p^{\text{BS}}, p^{\text{UE}}$ in (44)–(45) should also be multiplied by the inefficiency $\frac{1}{\omega^{\text{BS}}}, \frac{1}{\omega^{\text{UE}}} \geq 1$ of the power amplifiers at the BS and UE, respectively. Consequently, it is more appropriate to define the energy efficiencies as*

$$\text{EE}_{\text{overall}}^{\text{DL}} = \frac{\mathcal{C}^{\text{DL}}}{\left(\frac{T_{\text{data}}^{\text{DL}}}{T_{\text{coher}}} + \alpha_1\right) \left(\frac{p^{\text{BS}}}{\omega^{\text{BS}}} + N\varrho + \zeta\right) + \alpha_2 \left(\frac{p^{\text{UE}}}{\omega^{\text{UE}}} + N\varrho + \zeta\right)} \quad (49)$$

$$\text{EE}_{\text{overall}}^{\text{UL}} = \frac{\mathcal{C}^{\text{UL}}}{\left(\frac{T_{\text{data}}^{\text{UL}}}{T_{\text{coher}}} + \alpha_3\right) \left(\frac{p^{\text{UE}}}{\omega^{\text{UE}}} + N\varrho + \zeta\right)}. \quad (50)$$

Note that the unit is still bits/Joule and that similar definitions have appeared in [42]–[44] among others. Since the term $N\varrho$ grows with N , the overall energy efficiency approaches zero as $N \rightarrow \infty$; thus, it is maximized at some finite N . Nevertheless, recent work in [45] shows that massive MIMO offers great energy savings also when the circuit power is taken into account. This is also illustrated numerically herein.

¹⁰This term can also model the overhead power consumption of the network as a whole, which enable comparison of network architectures with different BS density, amounts of backhaul signaling, etc.

The power scaling laws in Corollary 6 are in fact SNR scaling laws. For fixed transmit powers, we can thus increase the transmission range by letting $\text{tr}(\mathbf{R})$ reduce proportionally to \sqrt{N} , instead of decreasing the transmit powers. Alternatively, we can *increase* the receiver noise powers σ_{BS}^2 and σ_{UE}^2 proportionally to \sqrt{N} . The receiver noise power is typically a product of the ideal thermal noise power and the noise figure, which describes the noise amplification caused by components in the receiver hardware. By increasing the number of antennas N , we can thus tolerate less ideal receiver hardware.

The ability to degrade the hardware quality with N can be taken even further. Recall from Section IV that the impact of hardware impairments at the BS vanishes as $N \rightarrow \infty$. This fact raises the important question: Can we increase the levels of impairments at the BS as N grows and still obtain non-zero capacities? The answer is given by the following corollary.

Corollary 7. *Suppose the levels of impairments $\kappa_t^{\text{BS}}, \kappa_r^{\text{BS}}$ are increased proportionally to N^{τ_t} and N^{τ_r} , respectively. The lower capacity bounds in Corollaries 4 and 5 (with $n \leq \frac{1}{2}$) converge to non-zero quantities as $N \rightarrow \infty$ if $\tau_r < \frac{1}{2}$ in the UL while $\tau_t + \tau_r < 1$ and $\tau_r < \frac{1}{2}$ in the DL.*

Proof: The proof is given in Appendix B-F. ■

This corollary shows that we can indeed increase the levels of impairments $\kappa_t^{\text{BS}}, \kappa_r^{\text{BS}}$ at the BS roughly proportionally to \sqrt{N} and still obtain non-zero asymptotic capacity. In fact, the numerical results in the next subsection shows that only minor degradations of the lower capacity bounds appear when the scaling law in Corollary 7 is followed.

Recall from (5) that the conventional EVM measure of transceiver quality equals the square root of the κ -parameters [15], thus the EVM can be degraded proportionally to $N^{1/4}$. A high-quality antenna element at the BS with an EVM of 0.03 can thus be replaced by 256 low-quality antenna elements with an EVM of 0.12, while the loss in capacity is negligible. This is a very encouraging result, since it indicates that massive MIMO can be deployed with inexpensive/low-quality hardware at the BSs. Note that the ability to degrade the hardware quality with N comes in addition to all other benefits of massive MIMO, for example, the array gain and the decorrelation of user channels that is further discussed in the multi-cell context; see Section VI.

A. Numerical Illustrations

Next, we show numerically that the transmit powers or hardware quality can be decreased as N grows large with only minor degradations in spectral efficiency. Figs. 9–10 illustrate the power scaling law of Corollary 6. The DL and UL powers are $p^{\text{BS}} = p^{\text{UE}} = 4.44 \mu\text{J}$ per channel use¹¹ for $N = 1$ and then reduced by a factor $1/N^t$ for $t \in \{0, \frac{1}{4}, \frac{1}{2}, 1\}$. The noise covariances are normalized as $\sigma^2 = 1$ and $\mathbf{Q} = \mathbf{S} = \mathbf{I}$, while the channel covariance matrix \mathbf{R} is generated by the exponential correlation model in (17) with correlation coefficient $r = 0.7$ and scaled such that $\frac{N\sigma^2}{\text{tr}(\mathbf{R})} = \frac{\text{tr}(\mathbf{Q})}{\text{tr}(\mathbf{R})} = 0.0444 \mu\text{J}$, thus giving an SNR of 20 dB for $N = 1$. The levels of impairments are set to $\kappa_t^{\text{BS}} = \kappa_r^{\text{BS}} = \kappa_t^{\text{UE}} = \kappa_r^{\text{UE}} = 0.05^2$. For simplicity,

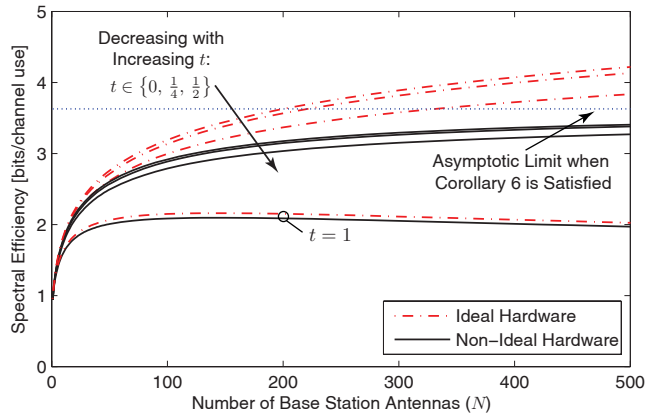


Fig. 9. Achievable spectral efficiency with ideal and non-ideal hardware when the transmit and pilot powers are reduced with N as $1/N^t$ for $t \in \{0, \frac{1}{4}, \frac{1}{2}, 1\}$. The results are valid for both DL and UL transmissions.

we select $(\alpha_1 + \alpha_2) \frac{T_{\text{coher}}}{T_{\text{data}}^{\text{DL}}} = 0.01$ and $\alpha_3 \frac{T_{\text{coher}}}{T_{\text{data}}^{\text{UL}}} = 0.01$, which gives identical EEs in the DL and UL.

Fig. 9 shows the DL/UL spectral efficiencies using the lower capacity bounds in Theorem 3. The figure verifies that these converge to non-zero asymptotic limits under non-ideal hardware. This holds even if the transmit power is reduced as $1/N^t$ for $t < \frac{1}{2}$. If we reduce the transmit power faster than the scaling law in Corollary 6 (e.g., $t = 1$), then the achievable spectral efficiencies will eventually reduce with N and approach zero. However, the decay is relatively slow (which can also be seen from the numerical results in [11]), which have an important impact in the next figure. The special case with ideal hardware gives a similar behavior for $t = 1$, while the spectral efficiencies grow without bound for $t < \frac{1}{2}$.

In Fig. 10, we show the achievable energy efficiency in the same scenario as in the previous figure. As expected from the discussion above, the EE with non-ideal hardware grows without bound as $N \rightarrow \infty$ for $t = \frac{1}{4}$ and $t = \frac{1}{2}$, while it converges to a finite value for $t = 0$ (i.e., when the transmit/pilot powers are fixed). However, the highest EE is achieved by $t = 1$ which does not satisfy the scaling law in Corollary 6. The spectral efficiency approaches zero as $N \rightarrow \infty$ in this scenario, but apparently at a much slower pace than the transmit power goes to zero. This means that if our primary goal is to achieve a high EE, we might as well reduce the power faster than the scaling law of Corollary 6.

Fig. 10 also shows the case with ideal hardware for comparison. Despite the fundamental differences when $N \rightarrow \infty$ or $p^{\text{BS}} \rightarrow \infty$ (i.e., there is no capacity ceiling or estimation error floor with ideal hardware), the difference in EE is quite small between ideal and non-ideal hardware; the relative performance loss for $t = \frac{1}{2}$ is 2–20% and increases with N .

Next, we consider the refined EE notion described in (49)–(50) of Remark 3. We fix the amplifier efficiencies at 40% (i.e., $\omega^{\text{BS}} = \omega^{\text{UE}} = 0.4$) and note that typical values of the static and per-antenna circuit power consumptions (per channel use) were $\zeta = 2.2 \mu\text{J}$ and $\rho = 0.08 \mu\text{J}$, respectively, in year

¹¹This corresponds to 40 W at an 9 MHz effective bandwidth.

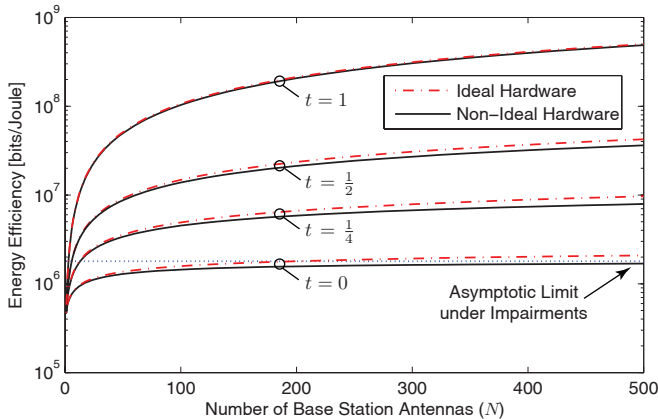


Fig. 10. Achievable energy efficiency with ideal and non-ideal hardware when the transmit and pilot powers are reduced with N as $1/N^t$ for $t \in \{0, \frac{1}{4}, \frac{1}{2}\}$. The EE is computed using the lower bounds in Theorem 3 and are valid for both DL and UL transmissions.

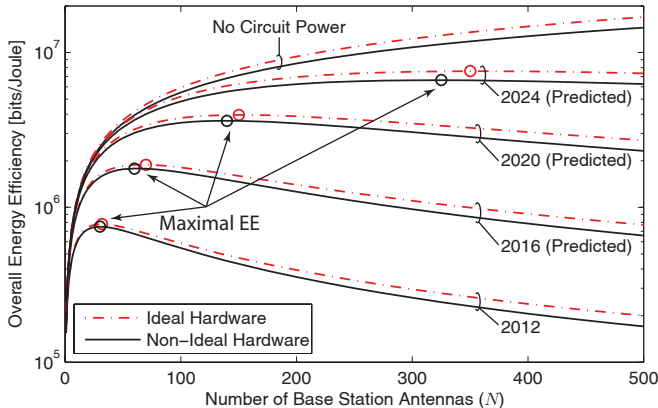


Fig. 11. Overall energy efficiency of ideal and non-ideal hardware when the transmit and pilot powers are reduced with N as $1/\sqrt{N}$. The amplifier efficiency is 40% and we consider predicted values of the static and per-antenna circuit power consumptions for different years. The numbers of antennas that maximize the overall EE are marked with rings.

2012 [46].¹² Assuming that these values reduce with 50% for every two years (i.e., in accordance to Moore's law), we can obtain simple predictions of the circuit power consumptions in the years 2016, 2020, and 2024. We also consider the case without any circuit power consumption as a reference. The corresponding overall EEs are shown in Fig. 11 for $t = \frac{1}{2}$ and the same propagation conditions as in the previous two figures. Several important observations can be made. First, the amplifier inefficiencies shift the curves downwards as compared to Fig. 10. Moreover, the EE is maximized at finite N and the optimal value seems to increase with time (i.e., with smaller values of ζ and ϱ). The figure indicates that massive MIMO with hundreds of antennas might not be an EE-optimal network architecture with the circuitry of today. However, our result also shows that massive MIMO systems can indeed promise very high EE in the near future. Clearly, the key to success is to decrease the part of the circuit power that scales with N .

¹²This corresponds to 19.9 W of static circuit power and 5.7 W of per-antenna circuit power (shared by 10 active users) at an 9 MHz effective bandwidth.

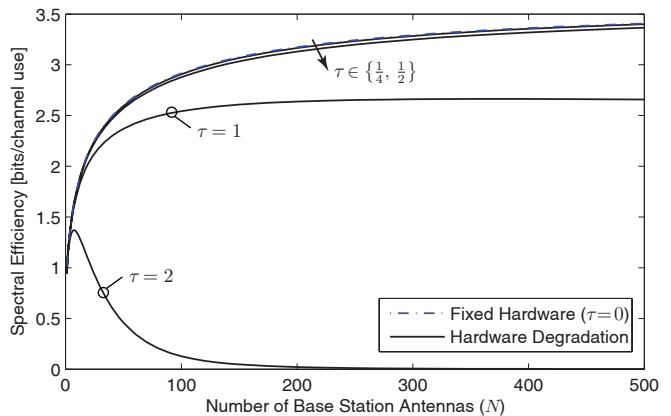


Fig. 12. Lower bounds on the capacity when the levels of impairments at the BS are increased with N as N^τ for $\tau \in \{0, \frac{1}{4}, \frac{1}{2}, 1, 2\}$. The results are valid for both DL and UL transmissions.

Finally, the ability to increase the levels of impairments at the BS is illustrated numerically. We consider a symmetric scenario with an average SNR of 20 dB in the DL and UL and $\frac{T_{\text{data}}^{\text{DL}}}{T_{\text{coher}}} = \frac{T_{\text{data}}^{\text{UL}}}{T_{\text{coher}}} = 0.45$, thus the DL and UL lower capacity bounds in Theorem 3 coincide. The channel covariance matrix \mathbf{R} is generated by the exponential correlation model in (17) with $r = 0.7$ and the noise covariances are $\sigma^2 = 1$ and $\mathbf{Q} = \mathbf{S} = \mathbf{I}$. We have $\kappa_t^{\text{UE}} = \kappa_r^{\text{UE}} = 0.05^2$ at the UE, while the levels of impairments at the BS are scaled as $\kappa_t^{\text{BS}} = \kappa_r^{\text{BS}} = 0.05^2 N^\tau$ for different τ -values: $\tau \in \{0, \frac{1}{4}, \frac{1}{2}, 1, 2\}$. The lower capacity bounds are shown in Fig. 12 as a function of N . The simulation confirms that the performance degradation is small when the scaling law in Corollary 7 is followed (e.g., for $\tau = \frac{1}{4}$ and $\tau = \frac{1}{2}$). A larger performance loss is observed for $\tau = 1$ and the curve begins to bend downwards at $N \approx 350$. In the extreme case of $N = 2$, the lower bound goes quickly to zero. While these asymptotic results are based on the lower capacity bounds, we note that whenever $\tau > 1$ the upper bounds in Corollaries 2 and 3 converge to zero as well.

VI. EXTENSIONS TO MULTI-CELL SCENARIOS

The asymptotic capacity analysis in Section IV, particularly the lower capacity bounds in Corollaries 4 and 5, are based on the assumptions $\mathbb{E}\{\sigma^2\} \leq \mathcal{O}(N^n)$ and $\mathbb{E}\{\sigma^2\} \leq \mathcal{O}(N^n)$ for some $n < 1$. Although the receiver noise variances will not scale with N (unless we change hardware components), we recall that σ^2 and \mathbf{Q} include interference from transmissions to/from other UEs which are treated as noise in the lower capacity bounds. The interference power might scale faster than assumed in Section IV, particularly under so-called pilot contamination which give rise to terms that scale as $\mathcal{O}(N)$ [7]–[11]. This section investigates the impact of inter-user interference in massive MIMO systems with non-ideal hardware. The BS and UE from the previous sections are referred to as the ones *under study*.

A. Inter-User Interference in the Uplink

To exemplify the impact of inter-user interference, we assume that there is a set \mathcal{U} of co-users that are scheduled for UL transmission in the current coherence period. These

co-users can be served by the BS under study or neighboring BSs, thus the number of co-users $|\mathcal{U}|$ is generally large. The block-fading channel from UE $l \in \mathcal{U}$ to the BS under study is modeled as $\mathbf{h}_l \sim \mathcal{CN}(\mathbf{0}, \mathbf{R}_l)$, where \mathbf{R}_l has bounded spectral norm and the channel is block fading. The co-user channels are assumed independent, which in practice means that users are selected to have no common scatterers [3], [4]—this is a basic criterion of spatial user separability in the scheduler. A more refined scheduling criteria would be the one in [47], where the coverage area is divided into location bins. The users in a bin are roughly equivalent in terms of channel statistics and should not be served simultaneously. Users in different bins have independent channels and sufficiently different spatial properties, thus selecting one user per location bin for parallel transmission is a reasonable scheduling decision.

The UL pilot signaling is limited to $T_{\text{pilot}}^{\text{UL}}$ channel uses in the TDD protocol depicted in Fig. 2. Since the number of co-users generally satisfies $|\mathcal{U}| > T_{\text{pilot}}^{\text{UL}}$, each pilot channel use must be allocated to multiple users. We divide \mathcal{U} into two disjoint sets: \mathcal{U}_{\parallel} are the users that send pilot symbols in parallel with the UE under study, while \mathcal{U}_{\perp} are the remaining users.¹³ The noise vector during UL pilot signaling becomes

$$\mathbf{v}_{\text{pilot}} = \boldsymbol{\xi} + \sum_{l \in \mathcal{U}_{\parallel}} d_l \mathbf{h}_l \quad (51)$$

where $\boldsymbol{\xi} \sim \mathcal{CN}(\mathbf{0}, \sigma_{\text{BS}}^2 \mathbf{I})$ is the receiver noise at the BS and d_l is the pilot symbol of UE $l \in \mathcal{U}_{\parallel}$. Assuming $|d_l|^2 = p^{\text{UE}}$, the noise covariance matrix during pilot signaling becomes

$$\mathbf{S} = \mathbb{E}\{\mathbf{v}_{\text{pilot}} \mathbf{v}_{\text{pilot}}^H\} = \sigma_{\text{BS}}^2 \mathbf{I} + p^{\text{UE}} \sum_{l \in \mathcal{U}_{\parallel}} \mathbf{R}_l. \quad (52)$$

The LMMSE estimator in Theorem 1 and the corresponding analysis in Section III holds for any \mathbf{S} , thus the explicit ways of computing $\mathbf{v}_{\text{pilot}}$, \mathbf{S} in (51)–(52) can be plugged in directly. The channel estimate $\hat{\mathbf{h}}$ is now correlated with the user channels \mathbf{h}_l for $l \in \mathcal{U}_{\parallel}$, which has important impact on the performance during data transmission. More specifically, the noise vector during UL data transmission becomes

$$\mathbf{v}_{\text{data}} = \boldsymbol{\xi} + \sum_{l \in \mathcal{U}} \mathbf{h}_l d_l \quad (53)$$

where $d_l \sim \mathcal{CN}(0, p^{\text{UE}})$ denotes the independent data signal sent by UE $l \in \mathcal{U}$. The noise covariance matrix during data transmission is

$$\mathbf{Q} = \mathbb{E}\{\mathbf{v}_{\text{data}} \mathbf{v}_{\text{data}}^H\} = \sigma_{\text{BS}}^2 \mathbf{I} + p^{\text{UE}} \sum_{l \in \mathcal{U}} \mathbf{h}_l \mathbf{h}_l^H. \quad (54)$$

Note that \mathbf{Q} depends on the current realization of the block-fading co-user channels and thus changes between coherence periods. The covariance matrix \mathbf{Q} has *not* bounded spectral norm; in fact, there are $|\mathcal{U}|$ eigenvalues of \mathbf{Q} that grow without bound as $N \rightarrow \infty$. This property affects the lower capacity bound in (34) of Theorem 3 where the noise term becomes

$$\mathbb{E}\{(\mathbf{v}^{\text{UL}})^H \mathbf{Q} \mathbf{v}^{\text{UL}} | \mathcal{B}^{\text{BS}}\} = \sigma_{\text{BS}}^2 + p^{\text{UE}} \sum_{l \in \mathcal{U}} \mathbb{E}\{|\mathbf{h}_l^H \mathbf{v}^{\text{UL}}|^2 | \mathcal{B}^{\text{BS}}\}. \quad (55)$$

¹³Only one pilot symbol is transmitted per UE in this section. For other pilot lengths $B > 1$, one can construct up to B parallel pilot signals that are orthogonal in space.

The following theorem shows how the interference terms $\mathbb{E}\{|\mathbf{h}_l^H \mathbf{v}^{\text{UL}}|^2 | \mathcal{B}^{\text{BS}}\}$ in (55) behave as N grows large.

Theorem 5. Assume no instantaneous CSI is utilized for decoding (i.e., $\mathcal{B}^{\text{BS}} = \mathcal{B}^{\text{UE}} = \emptyset$), interference is treated as receiver noise, and the receive combining vector $\mathbf{v} = \frac{\hat{\mathbf{h}}}{\|\hat{\mathbf{h}}\|_2}$. Under the noise/interference model in (51)–(54), the terms in (55) behave as

$$\begin{aligned} & \mathbb{E}\{|\mathbf{h}_l^H \mathbf{v}|^2\} \\ &= \begin{cases} \mathbb{E}\left\{\frac{p^{\text{UE}}(\text{tr}(\mathbf{A}\mathbf{R}_l))^2}{\text{tr}(\mathbf{A}(|d + \eta_t^{\text{UE}}|^2 \mathbf{R} + \boldsymbol{\Psi})\mathbf{A}^H)}\right\} + \mathcal{O}(\sqrt{N}), & l \in \mathcal{U}_{\parallel}, \\ \mathcal{O}(1), & l \in \mathcal{U}_{\perp}, \end{cases} \end{aligned} \quad (56)$$

where η_t^{UE} is random and $\mathbf{A}, \boldsymbol{\Psi}$ are given in Theorem 4.

The lower capacity bound in (43) is generalized by replacing the term $\mathcal{O}(\frac{1}{N^{1-\alpha}})$ in the denominator by

$$\begin{aligned} & \mathbb{E}\left\{\frac{\text{tr}(\mathbf{R} - \mathbf{C})}{\text{tr}(\mathbf{A}(|d + \eta_t^{\text{UE}}|^2 \mathbf{R} + \boldsymbol{\Psi})\mathbf{A}^H)}\right\} \sum_{l \in \mathcal{U}_{\parallel}} \left(\frac{\text{tr}(\mathbf{A}\mathbf{R}_l)}{\text{tr}(\mathbf{A}\mathbf{R})}\right)^2 \\ &+ \mathcal{O}\left(\frac{1}{N}\right). \end{aligned} \quad (57)$$

Proof: The proof is given in Appendix B-G. ■

This theorem shows that the effective interference from a co-user depends strongly on whether its pilot is sent in parallel or orthogonally to the UE under study. The interference from co-users in \mathcal{U}_{\perp} with orthogonal pilot transmission vanishes asymptotically since the user channels decorrelate with N , while the interference from co-users in \mathcal{U}_{\parallel} with parallel pilot transmission scales with N and remains. This is the very essence of pilot contaminated interference and Theorem 5 generalizes previous results from [7]–[11] (among others) to non-ideal hardware. The explanation to the diverse behavior in Theorem 5 is that the channel estimate $\hat{\mathbf{h}}$ used in the receive combining is independent of the co-user channels \mathbf{h}_l for $l \in \mathcal{U}_{\perp}$, but correlated with \mathbf{h}_l for $l \in \mathcal{U}_{\parallel}$ since these vectors appeared in the noise term (51) during pilot transmission.

Remark 4 (Mitigation of Pilot Contamination). *Pilot contamination is sometimes referred to as a fundamental limiting factor for the sum rate in cellular massive MIMO systems. However, this is not true under ideal hardware, which is easily seen from the fact that the capacity of single user transmission grows without bound as $N \rightarrow \infty$. This reveals that there exist scheduling algorithms that can eliminate the detrimental impact of pilot contamination (e.g., by gradually selecting fewer users as $N \rightarrow \infty$) and make sure that the sum rate grows without bound in cellular systems. The design of such scheduling algorithms for arbitrary system conditions is however an open problem.*

For any fixed number of users, the impact of pilot contamination can also be mitigated by making the users in \mathcal{U}_{\parallel} as spatially separated as possible (e.g., by making $\text{tr}(\mathbf{A}\mathbf{R}_l)$ in (57) small) [36], exploiting both pilots and data signals for semi-blind channel estimation [48], and making the TDD protocols in adjacent cells unsynchronized to avoid parallel pilot transmissions [49]. Note that [36], [48], [49] consider

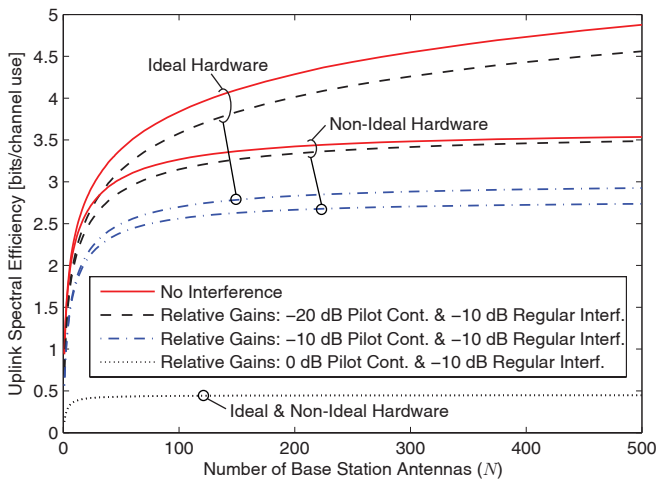


Fig. 13. Lower capacity bounds of a user that experiences regular inter-user interference and pilot contaminated interference. The loss in spectral efficiency depends strongly on the pilot contamination, while systems with non-ideal hardware are quite robust to regular inter-user interference.

ideal hardware, while we show in Section VI-C that pilot contamination is easily mitigated under non-ideal hardware.

B. Inter-User Interference in the Downlink

The downlink transmission can also suffer from pilot contamination, especially if the numbers of antennas at neighboring BSs also grow linearly with N . The interference and noise power take a similar form as in (53)–(55):

$$\sigma^2 = \sigma_{\text{UE}}^2 + p^{\text{BS}} \sum_{l \in \mathcal{U}} \mathbb{E} \left\{ |\tilde{\mathbf{h}}_l^H \mathbf{v}_l^{\text{DL}}|^2 | \mathcal{B}^{\text{BS}} \right\} \quad (58)$$

where σ_{UE}^2 is the receiver noise variance, \mathbf{v}_l^{DL} is the beamforming vector for DL transmission to UE $l \in \mathcal{U}$ from its serving BS, and $\tilde{\mathbf{h}}_l$ is the cross-channel from that BS to the UE under study. For brevity, we will not dive into the details since these require assumptions on the decision making at other BSs. The general behavior is however the same: UEs with parallel UL pilots cause non-vanishing interference to each other in the DL, while the impact of all other interfering DL transmissions vanish as N grows large.

C. Numerical Illustrations

The impact of inter-user interference and pilot contamination is now be analyzed numerically. We consider the lower bound on the UL capacity from Theorem 3 with $\mathbf{R} = \mathbf{I}$ and an SNR $p^{\text{UE}} \frac{\text{tr}(\mathbf{R})}{N\sigma_{\text{BS}}^2} = 20$ dB. We let $\frac{T_{\text{data}}^{\text{UL}}}{T_{\text{coher}}^{\text{UL}}} = 0.45$. Based on Theorem 5, we consider two different types of inter-user interference: regular interference from one UE with orthogonal pilot and pilot contaminated interference from another UE.

Fig. 6 shows the achievable UL spectral efficiency of the user under study with ideal hardware and non-ideal hardware with $\kappa_t^{\text{UE}} = \kappa_r^{\text{BS}} = 0.05^2$. The regular inter-user interference comes from a co-user with 10 dB weaker channel than the useful channel, while we consider three different cases for the pilot contaminated channel: it is 20, 10, or 0 dB weaker than the useful channel. The special case without any inter-user interference is given as a reference. Fig. 13 shows that weak

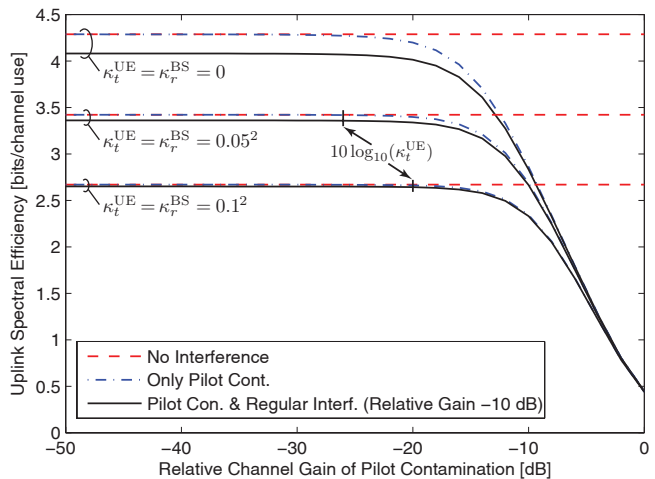


Fig. 14. Lower capacity bounds of a user that experiences pilot contaminated interference of varying strength and possibly regular inter-user interference that is -10 dB weaker than the useful channel. The interference drowns in the distortion noise if it is weaker than the level of impairments at the UE.

pilot contaminated interference has little impact, while the performance degradation is huge when the pilot contaminated channel is as strong as the useful channel. Furthermore, the ideal hardware case is more sensitive to interference than the non-ideal case. This is particularly evident when it comes to regular inter-user interference, which gives a much larger performance gap in the ideal case. As noted in Section IV-C, the gain of increasing the number of antennas beyond $N = 100$ is relatively small in the non-ideal case, but there is a larger incentive to do so under inter-user interference since it helps suppressing the regular interference. For this reason, multi-cell systems can still benefit from very large numbers of antennas since it enables simultaneous transmission to more users without increasing the regular interference level.

Next, we consider a fixed number of antennas, $N = 200$, and investigate how the spectral efficiency depends on the strength of the pilot contaminated interference. We consider three levels of impairments: $\kappa_t^{\text{UE}} = \kappa_r^{\text{BS}} \in \{0, 0.05^2, 0.1^2\}$. The lower capacity bounds are shown without interference, with only pilot contaminated interference, and with both types of interference. The horizontal axis in Fig. 14 shows the performance as a function of the relative channel gain of the pilot contaminated interference (with respect to the useful channel). This figure shows that the pilot contaminated interference has a negligible impact when it is much weaker than the useful channel, but there are breaking points where the degradation effect suddenly becomes immense. Interestingly, the breaking points are close to $10 \log_{10}(\kappa_t^{\text{UE}})$; that is, how much weaker the distortion noise caused by the UE is compared to the useful signal. This is very intuitive if we compare the size of the distortion term $\kappa_t^{\text{UE}} \mathbb{E} \{ |\varphi|^2 \}$ in lower capacity bound in (43) with the interference term in (57).

Corollary 8. *The pilot contaminated interference is negligible, when N grows large, if*

$$\kappa_t^{\text{UE}} \gg \sum_{l \in \mathcal{U}_{\parallel}} \left(\frac{\text{tr}(\mathbf{A}\mathbf{R}_l)}{\text{tr}(\mathbf{A}\mathbf{R})} \right)^2. \quad (59)$$

This corollary shows that pilot contaminated interference drowns in the distortion noise under certain conditions, which are independent of the absolute SNRs but depend on relative SNR differences of the type $\text{tr}(\mathbf{A}\mathbf{R}_l)/\text{tr}(\mathbf{A}\mathbf{R})$. Since the distortion noise typically is 20–30 dB weaker than the useful signal, the same is needed for the pilot contaminated interference to make its impact negligible. This is not a big deal in cellular deployments; the scheduler should simply allocate different pilots within each cell and to closely located cell-edge users of neighboring cells.¹⁴ This is achieved by the pilot allocation algorithm in [36], but also by simple predefined cell sectorization or location bins. We also note that regular inter-user interference has a small impact in Fig. 14, even if the channel is only 10 dB weaker than the useful channel. In other words, it is easy to make the regular inter-user interference and the pilot contamination drown in the distortion noise in massive MIMO systems.

VII. STEPS TOWARDS A MORE REFINED CHANNEL MODEL WITH HARDWARE IMPAIRMENTS

Using the generalized channel model in Section II, we have shown that additive distortion noise limits the estimation accuracy and channel capacities. However, physical hardware has additional impairment characteristics that might further degrade the performance. Some of these are outlined in this section. The upper capacity bounds in Theorem 2 are valid even under these refinements, but the lower capacity bounds are typically reduced.

The influence of hardware impairments is usually reduced by estimation, calibration, and other types of analog and digital signal processing. These techniques cannot remove the distortions completely, but leave residual errors that can also be modeled as additive distortion noise (with smaller κ -parameters than in an uncalibrated system) [15] and by the refined characteristics described in this section.

A. Power Loss

The total emitted power in the DL is $p^{\text{BS}}(1 + \kappa_t^{\text{BS}})$ under hardware impairments, and not the usual p^{BS} , since distortions contribute a small amount of power. This is easily handled by increasing the receiver noise power σ_{UE}^2 by a factor $(1 + \kappa_t^{\text{BS}})$, but simulations in [18] show that it has negligible impact on the spectral efficiency. Nevertheless, this *power loss* will not vanish as $N \rightarrow \infty$, although the distortion noise caused by the BS will do so. The power loss in the UL is analogous.

It is worth noting that it is not straightforward to model the total emitted power since some impairment sources (e.g., nonlinearities) might actually reduce the emitted power. Since the emitted power in our model is always p^{BS} or p^{UE} , we have implicitly compensated for such reductions by increasing the input power to the amplifier.

¹⁴As an example, suppose $\mathbf{R} = \delta^{-3.7}\mathbf{I}$ and $\mathbf{R}_l = \delta_l^{-3.7}\mathbf{I}$ where 3.7 is the path loss exponent and δ, δ_l are the distances between the BS under study and the two users. The right-hand side of (59) becomes $(\text{tr}(\mathbf{A}\mathbf{R}_l)/\text{tr}(\mathbf{A}\mathbf{R}))^2 = (\delta_l/\delta)^{-7.4}$ which is in the range -20 to -30 dB if UE l is 1.9–2.5 times further away from the BS than the UE under study. This is the case for most UEs in neighboring cells and the few co-users that do not satisfy this condition should be allocated orthogonal pilots.

B. High-Power Scalings

The levels of impairments in the transmitter hardware, $\kappa_t^{\text{BS}}, \kappa_t^{\text{UE}}$, generally depend on the transmit powers $p^{\text{BS}}, p^{\text{UE}}$ [17], [50]. These parameters are essentially constant within the dynamic range of the respective power amplifiers, but can increase rapidly outside these ranges due to non-linearities. This behavior was accurately modeled by polynomials in [17], [50]; for example, κ_t^{BS} could have a constant term describing the low-power EVM and a term $(p^{\text{BS}}/c)^q$ for some exponent q describing the severity/order of the non-linearities and a constant $c > 0$ that marks the end of the dynamic range [17]. Note that the distortion noise added by the low-noise amplifiers in radio receivers will typically not become worse with the received power, thus $\kappa_r^{\text{BS}}, \kappa_r^{\text{UE}}$ can be taken as constants.

Since the severity of impairments increases with the transmit powers, the capacity and estimation accuracy are not monotonically increasing with $p^{\text{BS}}, p^{\text{UE}}$ when using non-ideal hardware [50]. Since the high-power regime is not our main focus, $\kappa_t^{\text{BS}}, \kappa_t^{\text{UE}}$ have been taken as constants herein. Consequently, the high-power limits that we derived are optimistic and might not be achievable in practice—alternatively, they are the result of decreasing the propagation distance instead of increasing the power. The results when $N \rightarrow \infty$ are however accurate since $p^{\text{BS}}, p^{\text{UE}}$ are constants, or even decreased with N as in Section V.

C. Inter-Antenna Correlation for Distortion Noise

The distortion covariance matrices in (3) and (8) assume independent distortion between BS antennas. This implies that the distortion noise has a different spatial signature than the useful signal, which is the reason why the detrimental impact of distortion noise caused by the BS vanishes as $N \rightarrow \infty$. The underlying assumption is sufficient decoupling of the hardware chains of different antennas. Nevertheless, there might exist cross-correlation since the same useful signal is transmitter/received over the array. Such correlation was predicted and characterized in [51] but is typically small, thus we believe that the distortion noise and useful signal have different spatial signatures as N grows large also in practice.

D. Multiplicative Distortions

As described in Section II-B, our additive distortion model can accurately describe inter-carrier interference caused by phase noise and I/Q imbalance, as well as amplitude-amplitude nonlinearities in power amplifiers and quantization errors [14], [24], [25]. In addition to distortion noise, hardware impairments cause channel attenuations and phase shifts that are more appropriately modeled as multiplications with the channel vector \mathbf{h} . Some of these multiplicative distortions are relatively static and can be included in the channel vector \mathbf{h} by an appropriate scaling of the covariance matrix \mathbf{R} or by exploiting that the channel distribution is circularly symmetric. However, phase noise is a prime example of an impairment that causes multiplicative distortions that drift and accumulate within the channel coherence period [20], [52]–[54].

The true channel under phase noise can be described as $\text{diag}(e^{j\phi_{1,t}}, \dots, e^{j\phi_{N,t}})\mathbf{h}$, where j denotes the imaginary number and $\{\phi_{i,t}\}$ is the random process at the i th channel element. The phase drift is commonly modeled as a Wiener process

$$\phi_{i,t} = \phi_{i,t-1} + \theta_{i,t}^{\text{BS}} + \theta_t^{\text{UE}} \quad \forall i \quad (60)$$

where the initial value is $\phi_{i,0} = 0$ since $t = 0$ denotes the time of the channel estimation. The innovations that occurs t channel uses after the channel estimation are $\theta_{i,t}^{\text{BS}} \sim \mathcal{N}(0, \Delta^{\text{BS}})$ and $\theta_t^{\text{UE}} \sim \mathcal{N}(0, \Delta^{\text{UE}})$ at the BS and UE, respectively. Note that the single-antenna UE causes identical drifts on all channel elements, while the BS can cause identical or independent drifts depending on the use of a common oscillator (CO) or separate oscillators (SOs) at each antenna element. The phase drifts are temporally white, thus $\phi_{i,t} \sim \mathcal{N}(0, t\Delta^{\text{BS}} + t\Delta^{\text{UE}})$ which shows that the variance increases with time.

To comprehend the impact of phase noise, we note that the signal part of the received UL signal under MRC, $\mathbf{v} = \frac{\hat{\mathbf{h}}}{\|\hat{\mathbf{h}}\|_2}$, is

$$\begin{aligned} \mathbf{v}^H \text{diag}(e^{j\phi_{1,t}}, \dots, e^{j\phi_{N,t}})\mathbf{h}d \\ \approx \underbrace{\mathbf{v}^H \mathbf{h}d}_{\text{Ideal signal}} - \underbrace{j\mathbf{v}^H \text{diag}(\phi_{1,t}, \dots, \phi_{N,t})\mathbf{h}d}_{\text{Distortion from phase noise}} \end{aligned} \quad (61)$$

using the Taylor approximation $e^{j\phi_{i,t}} \approx 1 - j\phi_{i,t}$ because the drifts are small¹⁵ [55], [56]. The first term in (61) is the same as without phase noise, while the second term characterizes the mismatch from phase drift. A worst-case assumption would be to treat the second term as independent additive interference. This interference has zero mean and the variance is

$$\begin{aligned} & \mathbb{E} \left\{ \left| j\mathbf{v}^H \text{diag}(\phi_{1,t}, \dots, \phi_{N,t})\mathbf{h}d \right|^2 \right\} \\ &= \sum_{i_1=1}^N \sum_{i_2=1}^N \mathbb{E}\{v_{i_1}^* v_{i_2} h_{i_1} h_{i_2}^*\} \mathbb{E}\{\phi_{i_1,t} \phi_{i_2,t}^*\} \mathbb{E}\{|d|^2\} \\ &= p^{\text{UE}} \mathbb{E}\{|\mathbf{v}^H \mathbf{h}|^2\} t \Delta^{\text{UE}} \\ &+ \begin{cases} p^{\text{UE}} t \Delta^{\text{BS}} \mathbb{E}\{|\mathbf{v}^H \mathbf{h}|^2\}, & \text{if CO,} \\ p^{\text{UE}} t \Delta^{\text{BS}} \sum_{i=1}^N \mathbb{E}\{|h_i|^2 |v_i|^2\}, & \text{if SO,} \end{cases} \end{aligned} \quad (62)$$

where the first term originates from the UE and the second term is due to the BS having either a CO or a SO at each antenna. Recall from Theorem 4 that $\mathbb{E}\{|\mathbf{v}^H \mathbf{h}|^2\} = \mathcal{O}(N)$ and $\mathbb{E}\{|h_i|^2 |v_i|^2\} = \mathcal{O}(1)$. This means that a BS with a CO causes interference that scales as $\mathcal{O}(tN)$, while it only scales as $\mathcal{O}(t)$ when having SOs.¹⁶ In other words, it is preferable to have independent oscillators at each antenna element in massive MIMO systems, which was also noted in [20]. This is consistent with our results for additive distortion noise: impairments at the UE are N times more influential on the capacity, thus we can degrade the quality of the BS's oscillators with N with only a minor loss in performance. This is also positive for distributed massive MIMO deployments where the antenna separation is large and prevents the use of

¹⁵Since the variance of $\phi_{i,t}$ increases linearly with t , the Taylor approximation is only valid for a certain time. The time dependence can however be mitigated by tracking the phase noise within each coherence period [55].

¹⁶Since the useful signal power $p^{\text{UE}} \mathbb{E}\{|\mathbf{v}^H \mathbf{h}|^2\}$ also scales as $\mathcal{O}(N)$, the relative interference power behaves as $\mathcal{O}(t)$ with CO and $\mathcal{O}(t/N)$ with SOs.

a CO. A major difference from additive distortion noise is that the interference in (62) increases linearly with the time t , thus it eventually grow large and it becomes necessary to send pilot/calibration signals more often to mitigate it [20]. The phase noise process can also be tracked at the receiver, for example, by using previous received signals (see [55] and references therein). The tracking might be more accurate with a CO since then there are N observations of a single phase drift parameter.

Another important aspect of phase noise is that the standard deviations $\sqrt{\Delta^{\text{BS}}}$ and $\sqrt{\Delta^{\text{UE}}}$ typically scales with the carrier frequency [53], thus phase noise might be a major challenge in higher frequency bands (e.g., mmWave) [57].

E. Imperfect Channel Reciprocity

The downlink beamforming in massive MIMO TDD systems relies on channel reciprocity; that is, if \mathbf{h} is the uplink channel then \mathbf{h}^T is the downlink channel. This property holds for the radio-frequency propagation channels, but different transceiver chains are used for transmission/reception at the BS and the UE. The true downlink channel is therefore $\mathbf{h}^T \mathbf{D}_b$ where the diagonal matrix $\mathbf{D}_b = \text{diag}(b_1, \dots, b_N)$ contains N calibration parameters that are $b_i = 1 \forall i$ for ideal hardware but generally satisfies $b_i \neq 1 \forall i$ due to non-ideal hardware. The mismatch is fully specified by b_1, \dots, b_N and fortunately these parameters change slowly with time, thus one can compute estimates $\hat{b}_1, \dots, \hat{b}_N$ using a negligible amount of overhead signaling (even in massive MIMO systems [58]). Since the transmit beamforming mainly depends on the channel direction, it is often sufficient for the BS to compute the downlink channel up to an unknown scaling factor; see [16], [58]–[60] for different techniques that exploit uplink pilot transmissions. The estimates are naturally imperfect, thus $b_i = c(\hat{b}_i + e_i)$ where e_i is the estimation error and c is the unknown common scaling factor.

Imperfect channel reciprocity has no impact on the UL and is not changing anything fundamentally in the DL. There is a loss in received signal power since the beamforming direction is perturbed, but there is no self-interference since all the CSI available at the receiving UE is estimated in the downlink and thus reflects the true downlink channel $\mathbf{h}^T \mathbf{D}_b$. In other words, the lower capacity bound in (33) is still valid if we replace \mathbf{h} by $\mathbf{D}_b \mathbf{h}$ everywhere and compute the expectation with respect to the true distributions. The beamforming vector \mathbf{v}^{DL} is now a function of $\text{diag}(\hat{b}_1, \dots, \hat{b}_N) \hat{\mathbf{h}}$. This perturbation of \mathbf{v}^{DL} , as compared to having perfect reciprocity, behaves like channel estimation errors and is expected to vanish as N grows large. It should only have minor impact on the inter-user interference in multi-cell scenarios, since the reciprocity calibration errors are independent of the co-user channels.

VIII. CONCLUSION

This paper analyzed the capacity and estimation accuracy of massive MIMO systems with a new generalized channel model that includes distortion noises caused by transceiver hardware impairments. We proved analytically that the impairments in physical hardware create non-zero estimation error floors

and finite capacity ceilings in the uplink and downlink—irrespective of the SNR and number of base station antennas N . This stands in contrast to the very optimistic asymptotic results previously reported for ideal hardware. Despite these discouraging results, we showed that massive MIMO systems can still achieve a huge array gain, in the sense that an arbitrarily high energy efficiency can be obtained by decreasing the transmit powers as N grows. Furthermore, we proved that only the hardware impairments at the UEs limit the capacities as N grows large. This implies that the hardware quality at the BS can be decreased as N grows, which is an important insight and enabler for network deployments.

In multi-cell scenarios, we proved that the detrimental effect of inter-user interference and pilot contamination drowns in the distortion noise if a simple scheduling algorithm (e.g., classical sectorization) is used to avoid the strongest forms of pilot contaminated interference. In addition, we gave a brief description of how the generalized channel model considered in this paper can be refined to model hardware impairments in even greater detail and how such refinements would affect our results.

APPENDIX A

NEW AND OLD RESULTS ON RANDOM VECTORS

Lemma 2. [61, Eq. (2.2)] For invertible matrices \mathbf{B} and $\tau \in \mathbb{C}$, it holds that

$$(\mathbf{B} + \tau \mathbf{x} \mathbf{x}^H)^{-1} \mathbf{x} = \frac{\mathbf{B}^{-1} \mathbf{x}}{1 + \tau \mathbf{x} \mathbf{B}^{-1} \mathbf{x}^H}. \quad (63)$$

Lemma 3. Suppose $h \sim \mathcal{CN}(0, r)$ and $a, b > 0$, then

$$\mathbb{E} \left\{ \frac{|h|^2}{a|h|^2 + b} \right\} = \frac{1}{a} \left(1 - \frac{b}{ar} E_1 \left(\frac{b}{ar} \right) e^{\frac{b}{ar}} \right) \quad (64)$$

where $E_1(x) = \int_1^\infty \frac{e^{-tx}}{t} dt$ denotes the exponential integral.

Proof: Since $\rho = |h|^2$ has the exponential distribution with mean value r , the expectation in (64) equals

$$\int_0^\infty \frac{\rho}{a\rho + b} \frac{e^{-\rho/r}}{r} d\rho = \frac{b}{a^2 r} e^{\frac{b}{ar}} \int_1^\infty \left(1 - \frac{1}{x} \right) e^{-\frac{b}{ar} x} dx \quad (65)$$

where the equality follows from a change of variable $x = \frac{a}{b}\rho + 1$. Straightforward integration and identification of the exponential integral yield the right-hand side of (64). ■

Lemma 4. For any $a, b \in \mathbb{C}$ and non-zero $c, d \in \mathbb{C}$, we have

$$\left| \frac{a}{c} - \frac{b}{d} \right| \leq \frac{|b||c-d|}{|c||d|} + \frac{|a-b|}{|c|}. \quad (66)$$

Proof: This is straightforward to prove by using that $|ad - bc| = |ad - bc + bd - bd| \leq |b||c-d| + |d||a-b|$. ■

Lemma 5. Consider M arbitrary matrices $\mathbf{M}_1, \dots, \mathbf{M}_M \in \mathbb{C}^{N \times N}$ and an Hermitian positive semi-definite matrix $\mathbf{B} \in \mathbb{C}^{N \times N}$. It follows that

$$|\text{tr}(\mathbf{M}_1 \cdots \mathbf{M}_M \mathbf{B})| \leq \text{tr}(\mathbf{B}) \prod_{i=1}^M \|\mathbf{M}_i\|_2. \quad (67)$$

If $\mathbf{M}_1, \dots, \mathbf{M}_M, \mathbf{B}$ have uniformly bounded spectral norms, then

$$|\text{tr}(\mathbf{M}_1 \cdots \mathbf{M}_M \mathbf{B})| = \mathcal{O}(N). \quad (68)$$

Proof: The bound in (67) follows from that \mathbf{B} has non-negative eigenvalues and each matrix \mathbf{M}_i cannot amplify these by more than $\|\mathbf{M}_i\|_2$. The $\mathcal{O}(N)$ -scaling follows from (67) by using the assumptions and $\text{tr}(\mathbf{B}) \leq N \|\mathbf{B}\|_2$. ■

Lemma 6. [62, Lemma B.26] Let $\mathbf{B} \in \mathbb{C}^{N \times N}$ be deterministic and $\mathbf{x} = [x_1 \dots x_N]^T \in \mathbb{C}^N$ be a random vector of independent entries. Assume that $\mathbb{E}\{x_i\} = 0$, $\mathbb{E}\{|x_i|^2\} = 1$, and $\mathbb{E}\{|x_i|^\ell\} = \chi_\ell$. Then, for any $q \geq 1$,

$$\mathbb{E} \left\{ |\mathbf{x}^H \mathbf{B} \mathbf{x} - \text{tr}(\mathbf{B})|^q \right\} \leq C_q (\text{tr}(\mathbf{B} \mathbf{B}^H))^{\frac{q}{2}} (\chi_{\frac{q}{2}} + \chi_{2q}) \quad (69)$$

where C_q is a constant depending on q only.

Lemma 7. The channel estimate $\hat{\mathbf{h}}$ can be decomposed as

$$\hat{\mathbf{h}} = \mathbf{A} \left((d + \eta_t^{\text{UE}}) \mathbf{I} + \mathbf{D}_r \right) \mathbf{h} + \boldsymbol{\nu} \quad (70)$$

where \mathbf{A} is defined in (9) and the diagonal matrix \mathbf{D}_r has independent $\mathcal{CN}(0, \kappa_r^{\text{BS}} p^{\text{UE}})$ -entries such that $\boldsymbol{\eta}_r^{\text{BS}} = \mathbf{D}_r \mathbf{h}$.

For any realizations of η_t^{UE} and \mathbf{D}_r , the conditional distribution is

$$\hat{\mathbf{h}} | \eta_t^{\text{UE}}, \mathbf{D}_r \sim \mathcal{CN}(\mathbf{0}, \mathbf{A}(\boldsymbol{\Phi} + \mathbf{S})\mathbf{A}^H) \quad (71)$$

where $\boldsymbol{\Phi} = ((d + \eta_t^{\text{UE}}) \mathbf{I} + \mathbf{D}_r) \mathbf{R} ((d + \eta_t^{\text{UE}}) \mathbf{I} + \mathbf{D}_r)^H$.

Proof: This characterization follows directly from Theorem 1 and the channel model defined in Section II. ■

Lemma 8. For the channel \mathbf{h} and its estimate $\hat{\mathbf{h}}$ it holds that

$$\mathbb{E} \left\{ \left| \mathbf{h}^H \hat{\mathbf{h}} - (1 + d^{-1} \eta_t^{\text{UE}}) \text{tr}(\mathbf{R} - \mathbf{C}) \right|^2 \right\} = \mathcal{O}(N) \quad (72)$$

$$\mathbb{E} \left\{ \left| |\mathbf{h}^H \hat{\mathbf{h}}| - |1 + d^{-1} \eta_t^{\text{UE}}| \text{tr}(\mathbf{R} - \mathbf{C}) \right|^2 \right\} = \mathcal{O}(N). \quad (73)$$

Proof: Recall that $\hat{\mathbf{h}} = \mathbf{A}(\mathbf{h}(d + \eta_t^{\text{UE}}) + \boldsymbol{\nu} + \boldsymbol{\eta}_r^{\text{BS}})$ for $\mathbf{A} = d^* \mathbf{R} \mathbf{Z}^{-1}$. To prove (72), we expand the argument as

$$\begin{aligned} \left| \mathbf{h}^H \hat{\mathbf{h}} - (1 + d^{-1} \eta_t^{\text{UE}}) \text{tr}(\mathbf{R} - \mathbf{C}) \right|^2 &\leq 4 |\mathbf{h}^H \mathbf{A} \boldsymbol{\nu}|^2 \\ &+ 4 |\mathbf{h}^H \mathbf{A} \boldsymbol{\eta}_r^{\text{BS}}|^2 + 2 |d + \eta_t^{\text{UE}}|^2 |\mathbf{h}^H \mathbf{A} \mathbf{h} - d^{-1} \text{tr}(\mathbf{R} - \mathbf{C})|^2 \end{aligned} \quad (74)$$

by using the rule $|a + b|^q \leq 2^{q-1}(|a|^q + |b|^q)$ (from Hölder's inequality) twice. Next, we observe that

$$\begin{aligned} \mathbb{E}\{|\mathbf{h}^H \mathbf{A} \boldsymbol{\nu}|^2\} &= \text{tr}(\mathbf{A} \mathbf{S} \mathbf{A}^H \mathbf{R}) = \mathcal{O}(N) \\ \mathbb{E}\{|\mathbf{h}^H \mathbf{A} \boldsymbol{\eta}_r^{\text{BS}}|^2\} &= \kappa_r^{\text{BS}} p^{\text{UE}} \text{tr}(\mathbf{A} \mathbf{R}_{\text{diag}} \mathbf{A}^H \mathbf{R}) \end{aligned} \quad (75)$$

$$+ \kappa_r^{\text{BS}} p^{\text{UE}} \sum_{i=1}^N |\mathbf{e}_i^H \mathbf{R} \mathbf{A} \mathbf{e}_i|^2 = \mathcal{O}(N) \quad (76)$$

where \mathbf{e}_i is the i th column of an $N \times N$ identity matrix. The expression (75) follows from the independence of $\mathbf{h}, \boldsymbol{\nu}$ and (76) follows by straightforward computation using the characterization $\boldsymbol{\eta}_r^{\text{BS}} = \mathbf{D}_r \mathbf{h}$ in Lemma 7. The $\mathcal{O}(N)$ -properties follows from Lemma 5 since $\mathbf{R}, \mathbf{S}, \mathbf{A}$ have uniformly bounded spectral norms (by assumption).

Since $\mathbf{h} \sim \mathbf{R}^{1/2} \tilde{\mathbf{h}}$ for $\tilde{\mathbf{h}} \sim \mathcal{CN}(\mathbf{0}, \mathbf{I})$ and $d^{-1} \text{tr}(\mathbf{R} - \mathbf{C}) = \text{tr}(\mathbf{R}^{1/2} \mathbf{A} \mathbf{R}^{1/2})$ we can apply Lemma 6 to obtain

$$\begin{aligned} & \mathbb{E} \left\{ |d + \eta_t^{\text{UE}}|^2 \left| \mathbf{h}^H \mathbf{A} \mathbf{h} - d^{-1} \text{tr}(\mathbf{R} - \mathbf{C}) \right|^2 \right\} \\ & \leq (1 + \kappa_t^{\text{UE}}) 2\chi_4 C_2 \text{tr}((\mathbf{R} - \mathbf{C})^2) = \mathcal{O}(N). \end{aligned} \quad (77)$$

We obtain (72) by combining (74)–(77). Expression (73) follows directly, since it is upper bounded similarly to (74). ■

Lemma 9. For the channel \mathbf{h} and its estimate $\hat{\mathbf{h}}$ it holds that

$$\mathbb{E} \left\{ \left| \|\hat{\mathbf{h}}\|_2^2 - \text{tr}(\mathbf{A}(|d + \eta_t^{\text{UE}}|^2 \mathbf{R} + \Psi) \mathbf{A}^H) \right|^2 \right\} = \mathcal{O}(N) \quad (78)$$

$$\mathbb{E} \left\{ \left| \|\hat{\mathbf{h}}\|_2 - \sqrt{\text{tr}(\mathbf{A}(|d + \eta_t^{\text{UE}}|^2 \mathbf{R} + \Psi) \mathbf{A}^H)} \right|^2 \right\} = \mathcal{O}(1) \quad (79)$$

where \mathbf{A} is defined in (9) and $\Psi = p^{\text{UE}} \kappa_r^{\text{BS}} \mathbf{R}_{\text{diag}} + \mathbf{S}$.

Proof: By injecting the term $\text{tr}(\mathbf{A}(\Phi + \mathbf{S}) \mathbf{A}^H)$ from (71) and using the rule $|a + b|^q \leq 2^{q-1}(|a|^q + |b|^q)$ (from Hölder's inequality), we bound the left-hand side of (78) as

$$\begin{aligned} & \mathbb{E} \left\{ \left| \|\hat{\mathbf{h}}\|_2^2 - \text{tr}(\mathbf{A}(|d + \eta_t^{\text{UE}}|^2 \mathbf{R} + \Psi) \mathbf{A}^H) \right|^2 \right\} \\ & \leq 2\mathbb{E} \left\{ \left| \|\hat{\mathbf{h}}\|_2^2 - \text{tr}(\mathbf{A}(\Phi + \mathbf{S}) \mathbf{A}^H) \right|^2 \right\} \\ & + 2\mathbb{E} \left\{ \left| \text{tr}(\mathbf{A}(\Phi + \mathbf{S}) \mathbf{A}^H) - \text{tr}(\mathbf{A}(|d + \eta_t^{\text{UE}}|^2 \mathbf{R} + \Psi) \mathbf{A}^H) \right|^2 \right\} \end{aligned} \quad (80)$$

The first term in (80) satisfies

$$\begin{aligned} & \mathbb{E} \left\{ \left| \|\hat{\mathbf{h}}\|_2^2 - \text{tr}(\mathbf{A}(\Phi + \mathbf{S}) \mathbf{A}^H) \right|^2 \right\} \\ & \leq 4C_2 \mathbb{E} \left\{ \text{tr}(\mathbf{A}(\Phi + \mathbf{S}) \mathbf{A}^H \mathbf{A}(\Phi^H + \mathbf{S}^H) \mathbf{A}^H) \right\} \\ & \leq 4C_2 \|\mathbf{A}\|_2^4 \mathbb{E} \left\{ \|\Phi + \mathbf{S}\|_F^2 \right\} = \mathcal{O}(N) \end{aligned} \quad (81)$$

where the first inequality follows from applying Lemma 6 on (78) for fixed $\eta_t^{\text{UE}}, \mathbf{D}_r$ (note that the fourth-order moment is $\chi_4 = 2$ for complex Gaussian variables), while the second inequality follows from applying Lemma 5 twice. The scaling $\mathcal{O}(N)$ follows since $\|\mathbf{A}\|_2 = \mathcal{O}(1)$, $\|\mathbf{S}\|_F^2 = \mathcal{O}(N)$, $\mathbb{E}\{\text{tr}(\Phi \mathbf{S})\} \leq \|\mathbf{R}\|_2 \|\mathbf{S}\|_2 \mathbb{E}\{\|(d + \eta_t^{\text{UE}}) \mathbf{I} + \mathbf{D}_r\|_F^2\} = \mathcal{O}(N)$, and $\mathbb{E}\{\text{tr}(\Phi \Phi^H)\} \leq \|\mathbf{R}\|_2 \mathbb{E}\{\|(d + \eta_t^{\text{UE}}) \mathbf{I} + \mathbf{D}_r\|_F^2\} = \mathcal{O}(N)$ using Lemma 5.

Next, we characterize the second term in (80) as

$$\begin{aligned} & \mathbb{E} \left\{ \left| \text{tr}(\mathbf{A}(\Phi + \mathbf{S}) \mathbf{A}^H) - \text{tr}(\mathbf{A}(|d + \eta_t^{\text{UE}}|^2 \mathbf{R} + \Psi) \mathbf{A}^H) \right|^2 \right\} \\ & = \mathbb{E} \left\{ \left| \text{tr}(\mathbf{A}(\mathbf{D}_r \mathbf{R} \mathbf{D}_r^H + \mathbf{D}_r \mathbf{R} (d + \eta_t^{\text{UE}})^* \right. \right. \\ & \quad \left. \left. + (d + \eta_t^{\text{UE}}) \mathbf{R} \mathbf{D}_r^H) \mathbf{A}^H) - p^{\text{UE}} \kappa_r^{\text{BS}} \text{tr}(\mathbf{A} \mathbf{R}_{\text{diag}} \mathbf{A}^H) \right|^2 \right\} \\ & \leq 2\mathbb{E} \left\{ \left| \text{tr}(\mathbf{A}(\mathbf{D}_r \mathbf{R} \mathbf{D}_r^H - p^{\text{UE}} \kappa_r^{\text{BS}} \mathbf{R}_{\text{diag}}) \mathbf{A}^H) \right|^2 \right\} \end{aligned}$$

$$+ 4\mathbb{E} \left\{ |d + \eta_t^{\text{UE}}|^2 \right\} \mathbb{E} \left\{ \left| \text{tr}(\mathbf{A} \mathbf{D}_r \mathbf{R} \mathbf{A}^H) \right|^2 \right\} = \mathcal{O}(N). \quad (82)$$

where the equality follows from plugging in the expressions for Φ and Ψ and noting that the terms $|d + \eta_t^{\text{UE}}|^2 \text{tr}(\mathbf{A} \mathbf{R} \mathbf{A}^H)$ and $\text{tr}(\mathbf{A} \mathbf{S} \mathbf{A}^H)$ cancel out. The inequality follows again from the rule $|a + b|^q \leq 2^{q-1}(|a|^q + |b|^q)$. The $\mathcal{O}(N)$ -scaling follows since the first term in (82) is upper bounded by $(p^{\text{UE}} \kappa_r^{\text{BS}})^2 \text{tr}(\mathbf{A} \mathbf{R}_{\text{diag}} \mathbf{A}^H \mathbf{R}_{\text{diag}} \mathbf{A}^H) = \mathcal{O}(N)$ using Lemma 6 and some algebra, while $\mathbb{E}\{\left|\text{tr}(\mathbf{A} \mathbf{D}_r \mathbf{R} \mathbf{A}^H)\right|^2\} \leq \|\mathbf{R} \mathbf{A}^H \mathbf{A}\|_2^2 \mathbb{E}\{\left|\text{tr}(\mathbf{D}_r)\right|^2\} = \mathcal{O}(N)$ using Lemma 5. The expression (78) now follows from combining (80)–(82).

Finally, the expression (79) is proved as

$$\begin{aligned} & \mathbb{E} \left\{ \left| \|\hat{\mathbf{h}}\|_2 - \sqrt{\text{tr}(\mathbf{A}(|d + \eta_t^{\text{UE}}|^2 \mathbf{R} + \Psi) \mathbf{A}^H)} \right|^2 \right\} \\ & \leq \mathbb{E} \left\{ \frac{\left| \|\hat{\mathbf{h}}\|_2^2 - \text{tr}(\mathbf{A}(|d + \eta_t^{\text{UE}}|^2 \mathbf{R} + \Psi) \mathbf{A}^H) \right|^2}{\left| \|\hat{\mathbf{h}}\|_2 + \sqrt{\text{tr}(\mathbf{A}(|d + \eta_t^{\text{UE}}|^2 \mathbf{R} + \Psi) \mathbf{A}^H)} \right|^2} \right\} \\ & \leq \frac{\mathbb{E} \left\{ \left| \|\hat{\mathbf{h}}\|_2^2 - \text{tr}(\mathbf{A}(|d + \eta_t^{\text{UE}}|^2 \mathbf{R} + \Psi) \mathbf{A}^H) \right|^2 \right\}}{\text{tr}(\mathbf{A} \Psi \mathbf{A}^H)} = \mathcal{O}(1) \end{aligned} \quad (83)$$

where the first inequality follows from the rule $(a-b)(a+b) = a^2 - b^2$ and the second inequality is due to removal of non-zero terms from the denominator. The numerator and denominator have the same scaling which finalizes the proof of (79). ■

Lemma 10. For the estimated channel $\hat{\mathbf{h}}$ in (9) it holds that

$$\begin{aligned} & \mathbb{E} \left\{ \frac{|1 + d^{-1} \eta_t^{\text{UE}}|^k}{\|\hat{\mathbf{h}}\|_2^2} \right\} \leq \frac{2^k + 2^k \left(\frac{k}{2}\right)! (\kappa_t^{\text{UE}})^{\frac{k}{2}}}{\lambda_{\min}^+(\mathbf{B})(N_B - 1)} = \mathcal{O}(N^{-1}) \\ & \mathbb{E} \left\{ \frac{|1 + d^{-1} \eta_t^{\text{UE}}|^k}{\|\hat{\mathbf{h}}\|_2^4} \right\} \leq \frac{2^k + 2^k \left(\frac{k}{2}\right)! (\kappa_t^{\text{UE}})^{\frac{k}{2}}}{\lambda_{\min}^+(\mathbf{B})^2 (N_B - 1)(N_B - 2)} = \mathcal{O}(N^{-2}) \end{aligned} \quad (84)$$

for any even integer k , where $\lambda_{\min}^+(\mathbf{B}) > 0$ denotes the smallest non-zero eigenvalue of $\mathbf{B} = \mathbf{A} \mathbf{S} \mathbf{A}^H$ and $N_B = \text{rank}(\mathbf{B})$.

Proof: Using the conditional distribution of the channel estimate in (71), it holds for any integer $q > 0$ that

$$\begin{aligned} & \mathbb{E} \left\{ \frac{|1 + d^{-1} \eta_t^{\text{UE}}|^k}{\|\hat{\mathbf{h}}\|_2^{2q}} \right\} = \mathbb{E} \left\{ \mathbb{E} \left\{ \frac{|1 + d^{-1} \eta_t^{\text{UE}}|^k}{\|\hat{\mathbf{h}}\|_2^{2q}} \middle| \eta_t^{\text{UE}}, \mathbf{D}_r \right\} \right\} \\ & \leq \mathbb{E} \left\{ \frac{2^k (1 + |d^{-1} \eta_t^{\text{UE}}|^k)}{\lambda_{\min}^+(\mathbf{A} \mathbf{S} \mathbf{A}^H)^q} \right\} \mathbb{E} \left\{ \frac{1}{\|\mathbf{U}_B^H \mathbf{v}\|_2^{2q}} \right\} \end{aligned} \quad (86)$$

where the inequality follows from $\|\hat{\mathbf{h}}\|_2^2 = \mathbf{v}^H \mathbf{A}(\Phi + \mathbf{S}) \mathbf{A}^H \mathbf{v} \geq \mathbf{v}^H \mathbf{A} \mathbf{S} \mathbf{A}^H \mathbf{v} \geq \lambda_{\min}^+(\mathbf{A} \mathbf{S} \mathbf{A}^H) \|\mathbf{U}_B^H \mathbf{v}\|_2^2$ where $\mathbf{v} \sim \mathcal{CN}(\mathbf{0}, \mathbf{I})$ and $\mathbf{U}_B \in \mathbb{C}^{N \times N_B}$ is an orthogonal basis of the span of $\mathbf{A} \mathbf{S} \mathbf{A}^H$ (note that this matrix is generally rank-deficient). These expectations were separated since $\|\mathbf{U}_B^H \mathbf{v}\|_2^2$ is independent of the smallest non-zero eigenvalue. Furthermore, the rule $|a + b|^q \leq 2^q(|a|^q + |b|^q)$ from Hölder's inequality was applied on $|1 + d^{-1} \eta_t^{\text{UE}}|^k$. Note that $\mathbf{U}_B^H \mathbf{v} \sim \mathcal{CN}(\mathbf{0}, \mathbf{I})$ with a dimension reduced from N to N_B .

The final result in (84)–(85) follows from $\mathbb{E}\{|d^{-1}\eta_t^{\text{UE}}|^k\} = \left(\frac{k}{2}\right)!(\kappa_t^{\text{UE}})^{\frac{k}{2}}$ and that [63, Lemma 2.10] with $m = 1$ and $n = N_B$ gives

$$\mathbb{E}\left\{\frac{1}{\|\mathbf{U}_B^H \mathbf{v}\|_2^{2q}}\right\} = \begin{cases} \frac{1}{N_B-1}, & \text{if } q = 1, \\ \frac{1}{(N_B-1)(N_B-2)}, & \text{if } q = 2, \end{cases} \quad (87)$$

and that N_B scales linearly with N (see Section II).

APPENDIX B COLLECTION OF PROOFS

A. Proof of Lemma 1

The DL capacity in (19) is upper bounded as

$$C^{\text{DL}} \leq \frac{T_{\text{data}}^{\text{DL}}}{T_{\text{coher}}} \mathbb{E}\left\{\max_{\mathbf{w}(\mathbf{h}): \|\mathbf{w}\|_2=1} \log_2(1 + \text{SINR}(\mathbf{w}))\right\} \quad (88)$$

where

$$\text{SINR}(\mathbf{w}) = \frac{|\mathbf{h}^T \mathbf{w}|^2}{\kappa_t^{\text{BS}} \sum_{i=1}^N |h_i w_i|^2 + \kappa_r^{\text{UE}} |\mathbf{h}^T \mathbf{w}|^2 + \frac{\sigma_{\text{UE}}^2}{p^{\text{BS}}}} \quad (89)$$

by assuming that the interference part of n is somehow canceled, perfect CSI is available, and exploiting the corresponding optimality of single-stream Gaussian signaling [2], [6]. We can write (89) as

$$\text{SINR}(\mathbf{w}) = \frac{\mathbf{w}^H \mathbf{h}^* \mathbf{h}^T \mathbf{w}}{\mathbf{w}^H (\kappa_t^{\text{BS}} \mathbf{D}_{|\mathbf{h}|^2} + \kappa_r^{\text{UE}} \mathbf{h}^* \mathbf{h}^T + \frac{\sigma_{\text{UE}}^2}{p^{\text{BS}}} \mathbf{I}) \mathbf{w}} \quad (90)$$

by utilizing $\mathbf{w}^H \mathbf{w} = 1$. Since the logarithm is a monotonically increasing function, the maximization in (88) can be applied onto $\text{SINR}(\mathbf{w})$. Using (90), this optimization is a generalized Rayleigh quotient problem and thus solved by

$$\mathbf{w} = \frac{(\kappa_t^{\text{BS}} \mathbf{D}_{|\mathbf{h}|^2} + \kappa_r^{\text{UE}} \mathbf{h}^* \mathbf{h}^T + \frac{\sigma_{\text{UE}}^2}{p^{\text{BS}}} \mathbf{I})^{-1} \mathbf{h}^*}{\|(\kappa_t^{\text{BS}} \mathbf{D}_{|\mathbf{h}|^2} + \kappa_r^{\text{UE}} \mathbf{h}^* \mathbf{h}^T + \frac{\sigma_{\text{UE}}^2}{p^{\text{BS}}} \mathbf{I})^{-1} \mathbf{h}^*\|_2} \quad (91)$$

which is equivalent to (23) by using Lemma 2. The DL capacity bound in (21) follows from plugging (91) into (90) (we also took the complex conjugate of the real-valued SINR expression to make it more consistent with the UL).

The UL capacity bound in (22) follows from [6] and by assuming that the interference part of ν is somehow canceled. We note that the uplink SINR with a receive combining vector \mathbf{w} is

$$\frac{\mathbf{w}^H \mathbf{h} \mathbf{h}^H \mathbf{w}}{\mathbf{w}^H (\kappa_t^{\text{UE}} \mathbf{h} \mathbf{h}^H + \kappa_r^{\text{BS}} \mathbf{D}_{|\mathbf{h}|^2} + \frac{\sigma_{\text{BS}}^2}{p^{\text{UE}}} \mathbf{I}) \mathbf{w}}. \quad (92)$$

The receiver combining vector in (24) maximizes (92) and achieves the upper bound in (22).

B. Proof of Theorem 2

The DL capacity bound in (21) can be rewritten as

$$\frac{T_{\text{data}}^{\text{DL}}}{T_{\text{coher}}} \mathbb{E}\left\{\log_2\left(1 + \frac{\mathbf{h}^H (\kappa_t^{\text{BS}} \mathbf{D}_{|\mathbf{h}|^2} + \frac{\sigma_{\text{UE}}^2}{p^{\text{BS}}} \mathbf{I})^{-1} \mathbf{h}}{1 + \kappa_r^{\text{UE}} \mathbf{h}^H (\kappa_t^{\text{BS}} \mathbf{D}_{|\mathbf{h}|^2} + \frac{\sigma_{\text{UE}}^2}{p^{\text{BS}}} \mathbf{I})^{-1} \mathbf{h}}\right)\right\} \quad (93)$$

using Lemma 2. This expression has the structure $m(\psi) = \log_2(1 + \frac{\psi}{1 + \kappa_r^{\text{UE}} \psi})$ where $\psi = \mathbf{h}^H (\kappa_t^{\text{BS}} \mathbf{D}_{|\mathbf{h}|^2} + \frac{\sigma_{\text{UE}}^2}{p^{\text{BS}}} \mathbf{I})^{-1} \mathbf{h}$. Since $m(\psi)$ is a concave function of ψ , we apply Jensen's inequality to achieve a new upper bound

$$C^{\text{DL}} \leq \frac{T_{\text{data}}^{\text{DL}}}{T_{\text{coher}}} \mathbb{E}\{m(\psi)\} \leq \frac{T_{\text{data}}^{\text{DL}}}{T_{\text{coher}}} m(\mathbb{E}\{\psi\}). \quad (94)$$

The upper bound in (25) follows from evaluating $\mathbb{E}\{\psi\}$ as

$$\begin{aligned} \mathbb{E}\{\psi\} &= \mathbb{E}\left\{\mathbf{h}^H (\kappa_t^{\text{BS}} \mathbf{D}_{|\mathbf{h}|^2} + \frac{\sigma_{\text{UE}}^2}{p^{\text{BS}}} \mathbf{I})^{-1} \mathbf{h}\right\} \\ &= \sum_{i=1}^N \mathbb{E}\left\{\frac{|h_i|^2}{\kappa_t^{\text{BS}} |h_i|^2 + \frac{\sigma_{\text{UE}}^2}{p^{\text{BS}}}}\right\} = G^{\text{DL}} \end{aligned} \quad (95)$$

where the expression for G^{DL} is obtained from Lemma 3 using $a = \kappa_t^{\text{BS}}$ and $b = \frac{\sigma_{\text{UE}}^2}{p^{\text{BS}}}$.

The closed-form upper bound on the UL capacity in (26) is derived analogously to the DL capacity bound.

C. Proof of Theorem 3

We use an approach from [5] to obtain the lower bound in (33). The DL capacity is obtained by maximization over the distribution $f(\mathbf{s})$, while any heuristic selection yields a lower bound. We assume a rank-one Gaussian codebook $\mathbf{s} = \mathbf{v}^* s$ where $s \sim \mathcal{CN}(0, p^{\text{BS}})$ is the data signal and \mathbf{v}^* is a unit-norm beamforming vector computed as a deterministic function of $\hat{\mathbf{h}}$. The mutual information $\mathcal{I}(s; y)$ in (19) then transforms into

$$\mathcal{I}(s; y) = h(s) - h(s|y) \quad (96)$$

where $h(\cdot)$ denotes differential entropy. Under the limiting assumptions above we have

$$h(s) = \log_2(\pi e p^{\text{BS}}). \quad (97)$$

Next, we make the limiting assumption that s is LMMSE estimated from y at the receiver using some instantaneous CSI denoted by \mathcal{A} , which equals \mathcal{B}^{UE} in Theorem 3. Based on classical estimation results [26], this gives an estimation error variance of $p^{\text{BS}} - \frac{|\mathbb{E}\{s^* y | \mathcal{A}\}|^2}{\mathbb{E}\{|y|^2 | \mathcal{A}\}}$ where

$$\mathbb{E}\{s^* y | \mathcal{A}\} = p^{\text{BS}} \mathbb{E}\{\mathbf{h}^T \mathbf{v}^* | \mathcal{A}\} \quad (98)$$

$$\begin{aligned} \mathbb{E}\{|y|^2 | \mathcal{A}\} &= p^{\text{BS}} (1 + \kappa_r^{\text{UE}}) \mathbb{E}\{|\mathbf{h}^T \mathbf{v}^*|^2 | \mathcal{A}\} \\ &+ p^{\text{BS}} \kappa_t^{\text{BS}} \sum_{i=1}^N \mathbb{E}\{|h_i|^2 |v_i|^2 | \mathcal{A}\} + \mathbb{E}\{\sigma^2 | \mathcal{A}\} \end{aligned} \quad (99)$$

are computed by first taking the expectation over the noise terms (using the covariance matrices of the distortion noises in (3)–(4)) and then over the channel. We now obtain the bound

$$h(s|y) \leq \log_2\left(\pi e \left(p^{\text{BS}} - \frac{|\mathbb{E}\{s^* y | \mathcal{A}\}|^2}{\mathbb{E}\{|y|^2 | \mathcal{A}\}}\right)\right) \quad (100)$$

by utilizing that a Gaussian distribution maximizes the differential entropy for any given estimation error variance [29]. By substituting (97) and (100) into (96) we obtain

$$\begin{aligned} \mathcal{I}(s; y) &\geq \log_2(\pi e p^{\text{BS}}) - \log_2\left(\pi e \left(p^{\text{BS}} - \frac{|\mathbb{E}\{s^* y | \mathcal{A}\}|^2}{\mathbb{E}\{|y|^2 | \mathcal{A}\}}\right)\right) \\ &= \log_2\left(1 + \frac{|\mathbb{E}\{s^* y | \mathcal{A}\}|^2}{p^{\text{BS}} \mathbb{E}\{|y|^2 | \mathcal{A}\} - |\mathbb{E}\{s^* y | \mathcal{A}\}|^2}\right) \end{aligned} \quad (101)$$

which is equivalent to (33) since $|\mathbb{E}\{\mathbf{h}^T \mathbf{v}^* | \mathcal{A}\}|^2 = |\mathbb{E}\{\mathbf{h}^H \mathbf{v} | \mathcal{A}\}|^2$ and $\mathbb{E}\{|\mathbf{h}^T \mathbf{v}^*|^2 | \mathcal{A}\} = \mathbb{E}\{|\mathbf{h}^H \mathbf{v}|^2 | \mathcal{A}\}$.

Next, the UL capacity bound in (34) is proved by first taking any \mathbf{v} as receive combining vector. This limiting assumption transforms the UL into a SISO channel. The remaining proof is then analog to the DL case above.

D. Proof of Theorem 4

We introduce the notation $\sqrt{\text{tr}(\mathbf{R} - \mathbf{C})} \varrho = \frac{\vartheta}{\sqrt{\gamma}}$ where

$$\vartheta = (1 + d^{-1} \eta_t^{\text{UE}}) \text{tr}(\mathbf{R} - \mathbf{C}) \quad (102)$$

$$\gamma = \text{tr}(\mathbf{A}(|d + \eta_t^{\text{UE}}|^2 \mathbf{R} + \mathbf{\Psi}) \mathbf{A}^H). \quad (103)$$

Starting with the equivalence in (37), we use the rule $a^2 - b^2 = (a + b)(a - b)$ to obtain

$$\begin{aligned} & \left| \mathbb{E} \left\{ \frac{\mathbf{h}^H \hat{\mathbf{h}}}{\|\hat{\mathbf{h}}\|_2} \right\}^2 - \left| \mathbb{E} \left\{ \frac{\vartheta}{\sqrt{\gamma}} \right\} \right|^2 \right| \\ &= \left| \mathbb{E} \left\{ \frac{\mathbf{h}^H \hat{\mathbf{h}}}{\|\hat{\mathbf{h}}\|_2} - \frac{\vartheta}{\sqrt{\gamma}} \right\} \right| \left| \mathbb{E} \left\{ \frac{\mathbf{h}^H \hat{\mathbf{h}}}{\|\hat{\mathbf{h}}\|_2} + \frac{\vartheta}{\sqrt{\gamma}} \right\} \right| \\ &\leq \mathbb{E} \left\{ \left| \frac{\mathbf{h}^H \hat{\mathbf{h}}}{\|\hat{\mathbf{h}}\|_2} - \frac{\vartheta}{\sqrt{\gamma}} \right| \right\} \left(\mathbb{E} \left\{ \left| \frac{\mathbf{h}^H \hat{\mathbf{h}}}{\|\hat{\mathbf{h}}\|_2} \right| \right\} + \left| \mathbb{E} \left\{ \frac{\vartheta}{\sqrt{\gamma}} \right\} \right| \right). \end{aligned} \quad (104)$$

In order to prove the first part of the theorem, we must show that right-hand side of (104) behaves as $\mathcal{O}(\sqrt{N})$. Using Cauchy-Schwartz inequality and that $\gamma \geq \text{tr}(\mathbf{A} \mathbf{\Psi} \mathbf{A}^H)$, we have

$$\begin{aligned} & \left| \mathbb{E} \left\{ \frac{\mathbf{h}^H \hat{\mathbf{h}}}{\|\hat{\mathbf{h}}\|_2} \right\} \right| + \left| \mathbb{E} \left\{ \frac{\vartheta}{\sqrt{\gamma}} \right\} \right| \\ &\leq \mathbb{E}\{\|\mathbf{h}\|_2\} + \left| \mathbb{E} \left\{ \frac{\vartheta}{\sqrt{\text{tr}(\mathbf{A} \mathbf{\Psi} \mathbf{A}^H)}} \right\} \right| = \mathcal{O}(\sqrt{N}) \end{aligned} \quad (105)$$

thus it remains to prove that the $\mathbb{E} \left\{ \left| \frac{\mathbf{h}^H \hat{\mathbf{h}}}{\|\hat{\mathbf{h}}\|_2} - \frac{\vartheta}{\sqrt{\gamma}} \right| \right\} = \mathcal{O}(1)$. To this end, we expand the expression using Lemma 4:

$$\begin{aligned} & \mathbb{E} \left\{ \left| \frac{\mathbf{h}^H \hat{\mathbf{h}}}{\|\hat{\mathbf{h}}\|_2} - \frac{\vartheta}{\sqrt{\gamma}} \right| \right\} \leq \mathbb{E} \left\{ \frac{|\mathbf{h}^H \hat{\mathbf{h}} - \vartheta|}{\|\hat{\mathbf{h}}\|_2} \right\} \\ &+ \text{tr}(\mathbf{R} - \mathbf{C}) \mathbb{E} \left\{ \frac{|1 + d^{-1} \eta_t^{\text{UE}}| |\|\hat{\mathbf{h}}\|_2 - \sqrt{\gamma}|}{\|\hat{\mathbf{h}}\|_2 \sqrt{\gamma}} \right\}. \end{aligned} \quad (106)$$

The first term in (106) is asymptotically bounded since

$$\mathbb{E} \left\{ \frac{|\mathbf{h}^H \hat{\mathbf{h}} - \vartheta|}{\|\hat{\mathbf{h}}\|_2} \right\} \leq \sqrt{\underbrace{\mathbb{E} \left\{ |\mathbf{h}^H \hat{\mathbf{h}} - \vartheta|^2 \right\}}_{\stackrel{(a)}{=} \mathcal{O}(N)}} \underbrace{\left\{ \frac{1}{\|\hat{\mathbf{h}}\|_2^2} \right\}}_{\stackrel{(b)}{=} \mathcal{O}(N^{-1})}} = \mathcal{O}(1) \quad (107)$$

where the expectation of the numerator and denominator are separated using Hölder's inequality, (a) follows from Lemma

8, and (b) from Lemma 10 with $k = 0$. The second term of (106) is upper bounded by

$$\begin{aligned} & \underbrace{\text{tr}(\mathbf{R} - \mathbf{C})}_{= \mathcal{O}(N)} \underbrace{\sqrt{\mathbb{E} \left\{ \frac{|1 + d^{-1} \eta_t^{\text{UE}}|^2}{\|\hat{\mathbf{h}}\|_2^2 \gamma} \right\}}}_{= \mathcal{O}(N^{-1})} \underbrace{\sqrt{\mathbb{E} \left\{ \left| \|\hat{\mathbf{h}}\|_2 - \sqrt{\gamma} \right|^2 \right\}}}_{= \mathcal{O}(1)} \\ &= \mathcal{O}(1) \end{aligned} \quad (108)$$

where Hölder's inequality was used to separate the expectations. The scaling of the first square root follows from Lemma 10 and that $\frac{1}{\gamma} \leq \frac{1}{\text{tr}(\mathbf{A} \mathbf{\Psi} \mathbf{A}^H)} = \mathcal{O}(N^{-1})$ for any realization of η_t^{UE} . The scaling of the second square root follows from Lemma 9. By plugging these scaling expressions into (104), we have proved (37).

Similarly, the equivalence in (38) follows if

$$\begin{aligned} & \mathbb{E} \left\{ \left| \frac{|\mathbf{h}^H \hat{\mathbf{h}}|^2}{\|\hat{\mathbf{h}}\|_2^2} - \frac{|1 + d^{-1} \eta_t^{\text{UE}}|^2 (\text{tr}(\mathbf{R} - \mathbf{C}))^2}{\gamma} \right| \right\} \\ &\leq (\text{tr}(\mathbf{R} - \mathbf{C}))^2 \mathbb{E} \left\{ \frac{|1 + d^{-1} \eta_t^{\text{UE}}|^2 |\|\hat{\mathbf{h}}\|_2^2 - \gamma|}{\|\hat{\mathbf{h}}\|_2^2 \gamma} \right\} \\ &+ \mathbb{E} \left\{ \frac{|\mathbf{h}^H \hat{\mathbf{h}}|^2 - |1 + d^{-1} \eta_t^{\text{UE}}|^2 (\text{tr}(\mathbf{R} - \mathbf{C}))^2|}{\|\hat{\mathbf{h}}\|_2^2} \right\} \end{aligned} \quad (109)$$

scales as $\mathcal{O}(\sqrt{N})$, where the inequality follows from Lemma 4. By applying Hölder's inequality on the first term, we obtain

$$\begin{aligned} & \frac{(\text{tr}(\mathbf{R} - \mathbf{C}))^2}{\text{tr}(\mathbf{A} \mathbf{\Psi} \mathbf{A}^H)} \underbrace{\sqrt{\mathbb{E} \left\{ \frac{|1 + d^{-1} \eta_t^{\text{UE}}|^4}{\|\hat{\mathbf{h}}\|_2^4} \right\}}}_{\stackrel{(b)}{=} \mathcal{O}(N^{-2})}} \underbrace{\sqrt{\mathbb{E} \left\{ \left| \|\hat{\mathbf{h}}\|_2^2 - \gamma \right|^2 \right\}}}_{\stackrel{(c)}{=} \mathcal{O}(N)}} \\ &= \mathcal{O}(\sqrt{N}) \end{aligned} \quad (110)$$

where (a) follows from $\frac{1}{\gamma} \leq \frac{1}{\text{tr}(\mathbf{A} \mathbf{\Psi} \mathbf{A}^H)} = \mathcal{O}(N^{-1})$ which is a deterministic upper bound, (b) is characterized by Lemma 10, and (c) follows from Lemma 9. The second term behaves as

$$\begin{aligned} & \sqrt{\underbrace{\mathbb{E} \left\{ \left| |\mathbf{h}^H \hat{\mathbf{h}}| - |1 + d^{-1} \eta_t^{\text{UE}}| \text{tr}(\mathbf{R} - \mathbf{C}) \right|^2 \right\}}_{\stackrel{(d)}{=} \mathcal{O}(N)}}} \\ &\times \sqrt{\underbrace{\mathbb{E} \left\{ \frac{2|\mathbf{h}^H \hat{\mathbf{h}}|^2}{\|\hat{\mathbf{h}}\|_2^4} \right\}}_{\stackrel{(e)}{=} \mathcal{O}(1)}} + \underbrace{\mathbb{E} \left\{ \frac{2|1 + d^{-1} \eta_t^{\text{UE}}|^2 (\text{tr}(\mathbf{R} - \mathbf{C}))^2}{\|\hat{\mathbf{h}}\|_2^4} \right\}}_{\stackrel{(f)}{=} \mathcal{O}(1)}}} \\ &= \mathcal{O}(\sqrt{N}) \end{aligned} \quad (111)$$

by using the rule $a^2 - b^2 = (a + b)(a - b)$ and Hölder's inequality. (d) is characterized by Lemma 8 and (f) by Lemma 10. Moreover, (e) follows since $\frac{|\mathbf{h}^H \hat{\mathbf{h}}|^2}{\|\hat{\mathbf{h}}\|_2^4} \leq \frac{\|\mathbf{h}\|_2^2}{\|\hat{\mathbf{h}}\|_2^2} = \mathcal{O}(1)$ by Cauchy-Schwartz inequality and that $\|\mathbf{h}\|_2^2, \|\hat{\mathbf{h}}\|_2^2$ have same asymptotic scaling. By plugging these scaling expressions into (109), we have proved (38).

Finally, the equivalence in (39) follows since

$$\begin{aligned}
& \left| \sum_{i=1}^N \mathbb{E}\{|h_i|^2 |v_i|^2\} - 0 \right| \stackrel{(a)}{=} \left| \mathbb{E} \left\{ \frac{\|\hat{\mathbf{h}}\|_4^2}{\|\hat{\mathbf{h}}\|_2^2} \sum_{i=1}^N |h_i|^2 \frac{\hat{h}_i^2}{\|\hat{\mathbf{h}}\|_4^2} \right\} \right| \\
& \stackrel{(b)}{\leq} \left| \mathbb{E} \left\{ \frac{\|\hat{\mathbf{h}}\|_4^2}{\|\hat{\mathbf{h}}\|_2^2} \sqrt{\sum_{i=1}^N |h_i|^4} \sqrt{\sum_{i=1}^N \frac{\hat{h}_i^4}{\|\hat{\mathbf{h}}\|_4^4}} \right\} \right| = \left| \mathbb{E} \left\{ \frac{\|\hat{\mathbf{h}}\|_4^2}{\|\hat{\mathbf{h}}\|_2^2} \|\mathbf{h}\|_4^2 \right\} \right| \\
& \stackrel{(c)}{\leq} \sqrt{\sqrt{\mathbb{E}\{\|\mathbf{h}\|_4^8\}} \mathbb{E}\{\|\hat{\mathbf{h}}\|_4^8\}} \mathbb{E} \left\{ \frac{1}{\|\hat{\mathbf{h}}\|_2^4} \right\} \stackrel{(d)}{=} \mathcal{O}(1) \quad (112)
\end{aligned}$$

where (a) follows from $|v_i|^2 = \frac{\hat{h}_i^2}{\|\hat{\mathbf{h}}\|_2^2}$ and by inserting the L_4 -norms $\|\hat{\mathbf{h}}\|_4^2$. The reason for this is that the vector $[\hat{h}_1^2 \dots \hat{h}_N^2]^T / \|\hat{\mathbf{h}}\|_4^2$ now has unit L_2 -norm, thus we apply Cauchy-Schwarz inequality in (b) to bound the sum by $\|\mathbf{h}\|_4^2$. Next, (c) is obtained by applying Hölder's inequality twice and (d) follows from that $\mathbb{E}\{\|\mathbf{h}\|_4^8\} = \mathcal{O}(N^2)$ and $\mathbb{E}\{\|\hat{\mathbf{h}}\|_4^8\} = \mathcal{O}(N^2)$ and $\mathbb{E}\left\{\frac{1}{\|\hat{\mathbf{h}}\|_2^4}\right\} = \mathcal{O}(N^{-2})$ from Lemma 10.

E. Proof of Corollary 6

We begin with the DL and note that the arguments of the expectations in (41) have deterministic upper bounds since

$$|\varphi| \leq \sqrt{\frac{\text{tr}(\mathbf{R} - \mathbf{C})}{p^{\text{UE}} \text{tr}(\mathbf{A}\mathbf{R}\mathbf{A}^H)}} \quad (113)$$

for any realization of η_t^{UE} . The dominated convergence theorem implies that we can take the limit $N \rightarrow \infty$ inside the expectations.¹⁷ Next, we observe that scaling the pilot power p^{UE} proportionally to $1/N^{t_{\text{UE}}}$ for some $t_{\text{UE}} > 0$ means that $N^{t_{\text{UE}}} p^{\text{UE}} \rightarrow B$ as $N \rightarrow \infty$ for some $0 < B < \infty$. Therefore, we have

$$N^{t_{\text{UE}}} \text{tr}(\mathbf{R} - \mathbf{C}) = N^{t_{\text{UE}}} p^{\text{UE}} \text{tr}(\mathbf{R}\bar{\mathbf{Z}}^{-1}\mathbf{R}) \rightarrow B \text{tr}(\mathbf{R}\mathbf{S}^{-1}\mathbf{R}) \quad (114)$$

$$N^{t_{\text{UE}}} \text{tr}(\mathbf{A}(|d + \eta_t^{\text{UE}}|^2 \mathbf{R} + \Psi)\mathbf{A}^H) \rightarrow B \text{tr}(\mathbf{R}\mathbf{S}^{-1}\mathbf{R}) \quad (115)$$

as $N \rightarrow \infty$. Using (114) and (115) and the dominated convergence theorem we obtain

$$\lim_{N \rightarrow \infty} |\mathbb{E}\{\varphi\}|^2 = \left| \mathbb{E} \left\{ \frac{(1 + d^{-1} \eta_t^{\text{UE}}) \sqrt{B \text{tr}(\mathbf{R}\mathbf{S}^{-1}\mathbf{R})}}{\sqrt{B \text{tr}(\mathbf{R}\mathbf{S}^{-1}\mathbf{R})}} \right\} \right|^2 = 1 \quad (116)$$

$$\lim_{N \rightarrow \infty} \mathbb{E}\{|\varphi|^2\} = \mathbb{E} \left\{ \frac{|1 + d^{-1} \eta_t^{\text{UE}}|^2 B \text{tr}(\mathbf{R}\mathbf{S}^{-1}\mathbf{R})}{B \text{tr}(\mathbf{R}\mathbf{S}^{-1}\mathbf{R})} \right\} = 1 + \kappa_t^{\text{UE}} \quad (117)$$

which holds for any $t_{\text{UE}} > 0$.

We want the noise term $\frac{\mathbb{E}\{\sigma^2\}}{p^{\text{BS}} \text{tr}(\mathbf{R} - \mathbf{C})} = \frac{\mathbb{E}\{\sigma^2\}}{p^{\text{UE}} p^{\text{BS}} \text{tr}(\mathbf{R}\bar{\mathbf{Z}}^{-1}\mathbf{R})}$ to vanish for $\mathbb{E}\{\sigma^2\} = \mathcal{O}(1)$, thus we need $\liminf_N p^{\text{UE}} p^{\text{BS}} \text{tr}(\mathbf{R}\bar{\mathbf{Z}}^{-1}\mathbf{R}) > 0$. This holds if $t_{\text{BS}} + t_{\text{UE}} = t_{\text{sum}} < 1$, since then $\frac{\mathbb{E}\{\sigma^2\}}{p^{\text{UE}} p^{\text{BS}} \text{tr}(\mathbf{R}\bar{\mathbf{Z}}^{-1}\mathbf{R})} = \mathcal{O}(1/N^{1-t_{\text{sum}}})$ because $\text{tr}(\mathbf{R}\bar{\mathbf{Z}}^{-1}\mathbf{R}) = \mathcal{O}(N)$.

Finally, we need the $\mathcal{O}(1/\sqrt{N})$ terms in (46) to still vanish as $N \rightarrow \infty$. Some careful but lengthy algebra reveals that

¹⁷To be strict, we first should multiply all terms in (41) by p^{UE} .

the $\mathcal{O}(N)$ properties in Lemmas 9–10 become $\mathcal{O}(N^{1-t_{\text{UE}}})$. The term $\mathcal{O}(1/\sqrt{N})$ in the numerator of (46) becomes $\mathcal{O}(1/N^{\frac{1}{2}-t_{\text{UE}}})$ while the $\mathcal{O}(1/\sqrt{N})$ in the denominator becomes $\mathcal{O}(1/N^{\frac{1}{2}-t_{\text{UE}}})$. These terms vanish if $t_{\text{UE}} < \frac{1}{2}$, which finishes the proof for the DL.

The proof for the UL is analogous since the uplink capacity bound in (43) has the same structure and contains the same expectations as the downlink capacity.

F. Proof of Corollary 7

Recall from the proof of Corollary 6 that the dominated convergence theorem can be applied, which means that we can take the limit $N \rightarrow \infty$ inside the expectations in the DL capacity bound of (41) and UL capacity bound of (43). If $\kappa_t^{\text{BS}}, \kappa_r^{\text{BS}}$ grows with N , we then obtain

$$\lim_{N \rightarrow \infty} |\mathbb{E}\{\varphi\}|^2 = \left| \mathbb{E} \left\{ \frac{(1 + d^{-1} \eta_t^{\text{UE}}) \sqrt{\text{tr}(\mathbf{R}\mathbf{R}_{\text{diag}}^{-1}\mathbf{R})}}{\sqrt{\text{tr}(\mathbf{R}\mathbf{R}_{\text{diag}}^{-1}\mathbf{R})}} \right\} \right|^2 = 1 \quad (118)$$

$$\lim_{N \rightarrow \infty} \mathbb{E}\{|\varphi|^2\} = \mathbb{E} \left\{ \frac{|1 + d^{-1} \eta_t^{\text{UE}}|^2 \text{tr}(\mathbf{R}\mathbf{R}_{\text{diag}}^{-1}\mathbf{R})}{\text{tr}(\mathbf{R}\mathbf{R}_{\text{diag}}^{-1}\mathbf{R})} \right\} = 1 + \kappa_t^{\text{UE}}. \quad (119)$$

In the DL, we further note that $\frac{\kappa_t^{\text{BS}} \sum_{i=1}^N \mathbb{E}\{|h_i|^2 |v_i|^2\}}{\text{tr}(\mathbf{R} - \mathbf{C})} = \mathcal{O}\left(\frac{\kappa_t^{\text{BS}} \kappa_r^{\text{BS}}}{N}\right)$ since $\kappa_r^{\text{BS}} \text{tr}(\mathbf{R} - \mathbf{C}) \rightarrow \text{tr}(\mathbf{R}\mathbf{R}_{\text{diag}}^{-1}\mathbf{R}) = \mathcal{O}(N)$ as $N \rightarrow \infty$. If this term should vanish asymptotically, it is sufficient that $\frac{\kappa_t^{\text{BS}} \kappa_r^{\text{BS}}}{N} \rightarrow 0$ which corresponds to the condition in the corollary. The corresponding condition for the UL is obtained analogously and gives $\frac{(\kappa_r^{\text{BS}})^2}{N} \rightarrow 0$.

Finally, we note that the noise terms (for $n \leq \frac{1}{2}$) and the $\mathcal{O}\left(\frac{1}{\sqrt{N}}\right)$ terms in (41) and (43) all behave as $\mathcal{O}\left(\frac{\kappa_r^{\text{BS}}}{\sqrt{N}}\right)$ or smaller, after some straightforward but lengthy algebra. These terms thus vanish under the condition $\tau_r < \frac{1}{2}$ stated in the corollary.

G. Proof of Theorem 5

The interference expressions in (56) are proved similar to Theorem 4. For the case $l \in \mathcal{U}_{\parallel}$ we have

$$\begin{aligned}
& \mathbb{E} \left\{ \left| \frac{|\mathbf{h}_l^H \hat{\mathbf{h}}|^2}{\|\hat{\mathbf{h}}\|_2^2} - \frac{p^{\text{UE}} a_l^2}{\gamma} \right| \right\} \leq \mathbb{E} \left\{ \frac{|\mathbf{h}_l^H \hat{\mathbf{h}}|^2 - p^{\text{UE}} a_l^2}{\|\hat{\mathbf{h}}\|_2^2} \right\} \\
& + \mathbb{E} \left\{ \frac{p^{\text{UE}} a_l^2 \left| \|\hat{\mathbf{h}}\|_2^2 - \gamma \right|}{\|\hat{\mathbf{h}}\|_2^2 \gamma} \right\} = \mathcal{O}(\sqrt{N}) \quad (120)
\end{aligned}$$

where $\gamma = \text{tr}(\mathbf{A}(|d + \eta_t^{\text{UE}}|^2 \mathbf{R} + \mathbf{\Psi})\mathbf{A}^H)$ and $a_l = \text{tr}(\mathbf{A}\mathbf{R}_l)$. This follows since the first term in (120) equals

$$\begin{aligned} & \mathbb{E} \left\{ \frac{\left| |\mathbf{h}_l^H \hat{\mathbf{h}}| - \sqrt{p^{\text{UE}} a_l} \right| \left| |\mathbf{h}_l^H \hat{\mathbf{h}}| + \sqrt{p^{\text{UE}} a_l} \right|}{\|\hat{\mathbf{h}}\|_2^2} \right\} \\ & \leq \underbrace{\sqrt{\mathbb{E} \left\{ \left| |\mathbf{h}_l^H \hat{\mathbf{h}}| - \sqrt{p^{\text{UE}} a_l} \right|^2 \right\}}}_{=\mathcal{O}(\sqrt{N})}} \underbrace{\sqrt{\mathbb{E} \left\{ \frac{\|\mathbf{h}_l\|_2^2}{\|\hat{\mathbf{h}}\|_2^2} + \frac{p^{\text{UE}} a_l^2}{\|\hat{\mathbf{h}}\|_2^4} \right\}}}_{=\mathcal{O}(1)}} \\ & = \mathcal{O}(\sqrt{N}) \end{aligned} \quad (121)$$

by using Hölder's inequality, Lemma 6, Cauchy-Schwartz inequality, and Lemma 10. The second term in (120) is also upper bounded by $\mathcal{O}(\sqrt{N})$ by using Hölder's inequality and that $a_l = \mathcal{O}(N)$, $\mathbb{E}\{\|\hat{\mathbf{h}}\|_2^2 - \gamma\} = \mathcal{O}(N)$ from Lemma 9, $\mathbb{E}\{\|\hat{\mathbf{h}}\|_2^{-4}\} = \mathcal{O}(N^{-2})$ from Lemma 10, and $\frac{1}{\gamma} \leq \frac{1}{\text{tr}(\mathbf{A}\mathbf{\Psi}\mathbf{A}^H)} = \mathcal{O}(N^{-1})$.

Next, the case $l \in \mathcal{U}_\perp$ in (56) follows from $\mathbb{E}\{|\mathbf{h}_l^H \mathbf{v}^{\text{UL}}|^2\} = \mathbb{E}\{(\mathbf{v}^{\text{UL}})^H \mathbf{R}_l \mathbf{v}^{\text{UL}}\} \leq \|\mathbf{R}_l\|_2 = \mathcal{O}(1)$ since \mathbf{h}_l and \mathbf{v}^{UL} are independent.

Finally, we note that the noise term in the denominator of (43) would be

$$\frac{\mathbb{E}\{\mathbf{v}^H \mathbf{Q} \mathbf{v}\}}{p^{\text{UE}} \text{tr}(\mathbf{R} - \mathbf{C})} = \sum_{l \in \mathcal{U}_\perp} \frac{p^{\text{UE}} \mathbb{E}\{|\mathbf{h}_l^H \mathbf{v}|^2\}}{p^{\text{UE}} \text{tr}(\mathbf{R} - \mathbf{C})} + \mathcal{O}\left(\sqrt{\frac{1}{N}}\right) \quad (122)$$

where the first term is equal to (57) by exploiting (56) and $\text{tr}(\mathbf{R} - \mathbf{C}) = \sqrt{p^{\text{UE}}} \text{tr}(\mathbf{A}\mathbf{R})$.

REFERENCES

- [1] E. Björnson, J. Hoydis, M. Kountouris, and M. Debbah, "Hardware impairments in large-scale MISO systems: Energy efficiency, estimation, and capacity limits," in *Proc. Int. Conf. Digital Signal Process. (DSP)*, 2013.
- [2] E. Telatar, "Capacity of multi-antenna Gaussian channels," *European Trans. Telecom.*, vol. 10, no. 6, pp. 585–595, 1999.
- [3] X. Gao, O. Edfors, F. Rusek, and F. Tufvesson, "Linear pre-coding performance in measured very-large MIMO channels," in *Proc. IEEE VTC Fall*, 2011.
- [4] J. Hoydis, C. Hoek, T. Wild, and S. ten Brink, "Channel measurements for large antenna arrays," in *Int. Symp. Wireless Commun. Systems (ISWCS)*, 2012.
- [5] M. Medard, "The effect upon channel capacity in wireless communications of perfect and imperfect knowledge of the channel," *IEEE Trans. Inf. Theory*, vol. 46, no. 3, pp. 933–946, 2000.
- [6] E. Björnson, P. Zetterberg, M. Bengtsson, and B. Ottersten, "Capacity limits and multiplexing gains of MIMO channels with transceiver impairments," *IEEE Commun. Lett.*, vol. 17, no. 1, pp. 91–94, 2013.
- [7] F. Rusek, D. Persson, B. Lau, E. Larsson, T. Marzetta, O. Edfors, and F. Tufvesson, "Scaling up MIMO: Opportunities and challenges with very large arrays," *IEEE Signal Process. Mag.*, vol. 30, no. 1, pp. 40–60, 2013.
- [8] T. Marzetta, "Noncooperative cellular wireless with unlimited numbers of base station antennas," *IEEE Trans. Wireless Commun.*, vol. 9, no. 11, pp. 3590–3600, 2010.
- [9] J. Jose, A. Ashikhmin, T. Marzetta, and S. Vishwanath, "Pilot contamination and precoding in multi-cell TDD systems," *IEEE Trans. Commun.*, vol. 10, no. 8, pp. 2640–2651, 2011.
- [10] J. Hoydis, S. ten Brink, and M. Debbah, "Massive MIMO in the UL/DL of cellular networks: How many antennas do we need?" *IEEE J. Sel. Areas Commun.*, vol. 31, no. 2, pp. 160–171, 2013.
- [11] H. Ngo, E. Larsson, and T. Marzetta, "Energy and spectral efficiency of very large multiuser MIMO systems," *IEEE Trans. Commun.*, vol. 61, no. 4, pp. 1436–1449, 2013.
- [12] J. Qi and S. Aissa, "On the power amplifier nonlinearity in MIMO transmit beamforming systems," *IEEE Trans. Commun.*, vol. 60, no. 3, pp. 876–887, 2012.
- [13] B. Maham and O. Tirkkonen, "Transmit antenna selection OFDM systems with transceiver IQ imbalance," *IEEE Trans. Veh. Technol.*, vol. 61, no. 2, pp. 865–871, 2012.
- [14] T. Schenk, *RF Imperfections in High-Rate Wireless Systems: Impact and Digital Compensation*. Springer, 2008.
- [15] C. Studer, M. Wenk, and A. Burg, "MIMO transmission with residual transmit-RF impairments," in *Proc. ITG/IEEE Workshop on Smart Antennas (WSA)*, 2010.
- [16] P. Zetterberg, "Experimental investigation of TDD reciprocity-based zero-forcing transmit precoding," *EURASIP J. on Adv. in Signal Process.*, Jan. 2011.
- [17] E. Björnson, P. Zetterberg, and M. Bengtsson, "Optimal coordinated beamforming in the multicell downlink with transceiver impairments," in *Proc. IEEE Global Commun. Conf. (GLOBECOM)*, 2012.
- [18] E. Björnson and E. Jorswieck, "Optimal resource allocation in coordinated multi-cell systems," *Foundations and Trends in Communications and Information Theory*, vol. 9, no. 2-3, pp. 113–381, 2013.
- [19] T. Koch, A. Lapidoth, and P. Sotiriadis, "Channels that heat up," *IEEE Trans. Inf. Theory*, vol. 55, no. 8, pp. 3594–3612, 2009.
- [20] A. Pitarokoulis, S. Mohammed, and E. Larsson, "Uplink performance of time-reversal MRC in massive MIMO systems subject to phase noise," *IEEE Trans. Wireless Commun.*, submitted, arXiv:1306.4495.
- [21] S. Mohammed and E. Larsson, "Per-antenna constant envelope precoding for large multi-user MIMO systems," *IEEE Trans. Commun.*, vol. 61, no. 3, pp. 1059–1071, 2013.
- [22] G. Caire, N. Jindal, M. Kobayashi, and N. Ravindran, "Multiuser MIMO achievable rates with downlink training and channel state feedback," *IEEE Trans. Inf. Theory*, vol. 56, no. 6, pp. 2845–2866, 2010.
- [23] E. Björnson, M. Kountouris, M. Bengtsson, and B. Ottersten, "Receive combining vs. multi-stream multiplexing in downlink systems with multi-antenna users," *IEEE Trans. Signal Process.*, vol. 61, no. 13, pp. 3431–3446, 2013.
- [24] H. Holma and A. Toskala, *LTE for UMTS: Evolution to LTE-Advanced*, 2nd ed. Wiley, 2011.
- [25] A. Mezghani, M.-S. Khoufi, and J. Nossek, "A modified MMSE receiver for quantized MIMO systems," in *Proc. ITG/IEEE Workshop on Smart Antennas (WSA)*, 2007.
- [26] S. Kay, *Fundamentals of Statistical Signal Processing: Estimation Theory*. Prentice Hall, 1993.
- [27] J. Kotecha and A. Sayeed, "Transmit signal design for optimal estimation of correlated MIMO channels," *IEEE Trans. Signal Process.*, vol. 52, no. 2, pp. 546–557, 2004.
- [28] E. Björnson and B. Ottersten, "A framework for training-based estimation in arbitrarily correlated Rician MIMO channels with Rician disturbance," *IEEE Trans. Signal Process.*, vol. 58, no. 3, pp. 1807–1820, 2010.
- [29] B. Hassibi and B. Hochwald, "How much training is needed in multiple-antenna wireless links?" *IEEE Trans. Inf. Theory*, vol. 49, no. 4, pp. 951–963, 2003.
- [30] N. O'Donoghue and J. Moura, "On the product of independent complex Gaussians," *IEEE Trans. Signal Process.*, vol. 60, no. 3, pp. 1050–1063, 2012.
- [31] J. Hoydis, M. Kobayashi, and M. Debbah, "Optimal channel training in uplink network MIMO systems," *IEEE Trans. Signal Process.*, vol. 59, no. 6, pp. 2824–2833, 2011.
- [32] S. Wagner, R. Couillet, M. Debbah, and D. Slock, "Large system analysis of linear precoding in MISO broadcast channels with limited feedback," *IEEE Trans. Inf. Theory*, vol. 58, no. 7, pp. 4509–4537, 2012.
- [33] S. Loyka, "Channel capacity of MIMO architecture using the exponential correlation matrix," *IEEE Commun. Lett.*, vol. 5, no. 9, pp. 369–371, 2001.
- [34] E. Björnson, D. Hammarwall, and B. Ottersten, "Exploiting quantized channel norm feedback through conditional statistics in arbitrarily correlated MIMO systems," *IEEE Trans. Signal Process.*, vol. 57, no. 10, pp. 4027–4041, 2009.
- [35] D. Shiu, G. Foschini, M. Gans, and J. Kahn, "Fading correlation and its effect on the capacity of multielement antenna systems," *IEEE Trans. Commun.*, vol. 48, no. 3, pp. 502–513, 2000.
- [36] H. Yin, D. Gesbert, M. Filippou, and Y. Liu, "A coordinated approach to channel estimation in large-scale multiple-antenna systems," *IEEE J. Sel. Areas Commun.*, vol. 31, no. 2, pp. 264–273, 2013.
- [37] A. Adhikary, J. Nam, J.-Y. Ahn, and G. Caire, "Joint spatial division and multiplexing," submitted, arXiv:1209.1402.

- [38] R. Couillet and M. Debbah, *Random Matrix Methods for Wireless Communications*. Cambridge University Press, 2011.
- [39] N. Shariati, E. Björnson, M. Bengtsson, and M. Debbah, "Low-complexity channel estimation in large-scale MIMO using polynomial expansion," in *Proc. IEEE PIMRC*, 2013.
- [40] G. Caire and S. Shamai, "On the capacity of some channels with channel state information," *IEEE Trans. Inf. Theory*, vol. 45, no. 6, pp. 2007–2019, 1999.
- [41] S. Verdú, "On channel capacity per unit cost," *IEEE Trans. Inf. Theory*, vol. 36, no. 5, pp. 1019–1030, 1990.
- [42] G. Auer, V. Giannini, C. Desset, I. Godor, P. Skillermark, M. Olsson, M. Imran, D. Sabella, M. Gonzalez, O. Blume, and A. Fehske, "How much energy is needed to run a wireless network?" *IEEE Wireless Commun. Mag.*, vol. 18, no. 5, pp. 40–49, 2012.
- [43] J. Xu, L. Qiu, and C. Yu, "Improving energy efficiency through multimode transmission in the downlink MIMO systems," *EURASIP J. Wirel. Commun. Netw.*, 2011.
- [44] D. Ng, E. Lo, and R. Schober, "Energy-efficient resource allocation in OFDMA systems with large numbers of base station antennas," *IEEE Trans. Wireless Commun.*, vol. 11, no. 9, pp. 3292–3304, 2012.
- [45] E. Björnson, M. Kountouris, and M. Debbah, "Massive MIMO and small cells: Improving energy efficiency by optimal soft-cell coordination," in *Proc. Int. Conf. Telecommun. (ICT)*, 2013.
- [46] G. Auer, O. Blume, V. Giannini, I. Godor, M. Imran, Y. Jading, E. Katranaras, M. Olsson, D. Sabella, P. Skillermark, and W. Wajda, *D2.3: Energy efficiency analysis of the reference systems, areas of improvements and target breakdown*. INFISO-ICT-247733 EARTH, ver. 2.0, 2012.
- [47] H. Huh, G. Caire, H. Papadopoulos, and S. Ramprasad, "Achieving "massive MIMO" spectral efficiency with a not-so-large number of antennas," *IEEE Trans. Wireless Commun.*, vol. 11, no. 9, pp. 3226–3239, 2012.
- [48] R. Müller, M. Vehkaperä, and L. Cottatellucci, "Blind pilot decontamination," in *Proc. ITG Workshop on Smart Antennas (WSA)*, 2013.
- [49] F. Fernandes, A. Ashikhmin, and T. Marzetta, "Inter-cell interference in noncooperative TDD large scale antenna systems," *IEEE J. Sel. Areas Commun.*, vol. 31, no. 2, pp. 192–201, 2013.
- [50] C. Studer, M. Wenk, and A. Burg, "System-level implications of residual transmit-RF impairments in MIMO systems," in *Proc. European Conf. Antennas and Propagation (EuCAP)*, 2011.
- [51] N. Moghadam, P. Zetterberg, P. Händel, and H. Hjalmarsson, "Correlation of distortion noise between the branches of MIMO transmit antennas," in *Proc. IEEE Int. Symp. Personal, Indoor and Mobile Radio Commun. (PIMRC)*, 2012.
- [52] A. Demir, A. Mehrotra, and J. Roychowdhury, "Phase noise in oscillators: A unifying theory and numerical methods for characterization," *IEEE Trans. Circuits Syst. I*, vol. 47, no. 5, pp. 655–674, 2000.
- [53] D. Petrovic, W. Rave, and G. Fettweis, "Effects of phase noise on OFDM systems with and without PLL: Characterization and compensation," *IEEE Trans. Commun.*, vol. 55, no. 8, pp. 1607–1616, 2007.
- [54] G. Durisi, A. Tarable, C. Camarda, and G. Montorsi, "On the capacity of MIMO Wiener phase-noise channels," in *Proc. Information Theory and Applications Workshop (ITA)*, 2013.
- [55] H. Mehrpouyan, A. Nasir, S. Blostein, T. Eriksson, G. Karagiannidis, and T. Svensson, "Joint estimation of channel and oscillator phase noise in MIMO systems," *IEEE Trans. Signal Process.*, vol. 60, no. 9, pp. 4790–4807, 2012.
- [56] Y. Nasser, M. Noes, L. Ros, and G. Jourdain, "On the system level prediction of joint time frequency spreading systems with carrier phase noise," *IEEE Trans. Commun.*, vol. 58, no. 3, pp. 839–850, 2010.
- [57] R. Baldemair, E. Dahlman, G. Fodor, G. Mildh, S. Parkvall, Y. Selen, H. Tullberg, and K. Balachandran, "Evolving wireless communications: Addressing the challenges and expectations of the future," *IEEE Veh. Technol. Mag.*, vol. 8, no. 1, pp. 24–30, 2013.
- [58] C. Shepard, H. Yu, N. Anand, L. Li, T. Marzetta, R. Yang, and L. Zhong, "Argos: Practical many-antenna base stations," in *Proc. ACM MobiCom*, 2012.
- [59] K. Nishimori, K. Cho, Y. Takatori, and T. Hori, "Automatic calibration method using transmitting signals of an adaptive array for TDD systems," *IEEE Trans. Veh. Technol.*, vol. 50, no. 6, pp. 1636–1640, 2001.
- [60] R. Rogalin, O. Bursalioğlu, H. Papadopoulos, G. Caire, and A. Molisch, "Downlink beamforming avoiding DOA estimation for cellular mobile communications," in *Proc. Information Theory and Applications Workshop (ITA)*, 2013.
- [61] J. Silverstein and Z. Bai, "On the empirical distribution of eigenvalues of a class of large dimensional random matrices," *J. Multivariate Analysis*, vol. 54, no. 2, pp. 175–192, 1995.
- [62] Z. Bai and J. Silverstein, *Spectral analysis of large dimensional random matrices*, 2nd ed. Springer Series in Statistics, 2009.
- [63] A. Tulino and S. Verdú, "Random Matrix Theory and Wireless Communications," *Foundations and Trends in Communications and Information Theory*, vol. 1, no. 1, pp. 1–182, 2004.